Non-equilibrium upscaling of compositional transport

Nanne Kuipéri

30 January 2018

Master of Science Thesis

TU Delft Delft University of Technology

Department of Geoscience and Engineering

Non-equilibrium upscaling of compositional transport

By

N. Kuipéri

in partial fulfilment of the requirements for the degree of

Master of Science
in Petroleum Engineering

at the Delft University of Technology,
to be defended publicly on Tuesday January 30, 2018 at 15:30 AM.

Supervisor:	Dr. D.V. Voskov	
Thesis committee:	Prof. Dr. W.R. Rossen,	TU Delft
	Prof. Dr. J. Bruining,	TU Delft
	Dr. J.E.A. Storms	TU Delft

Abstract

Reservoir simulation is a broadly used tool in the oil and gas production industry. It can be used for production history matching, performance forecasting and field development. A common Enhanced Oil Recovery (EOR) method is the injection of miscible gases. With the injection of gas into an oil reservoir, the system has to be considered as multiphase and multicomponent. Compositional simulation gives an accurate representation of the physics of multiphase and multicomponent systems. Solving the system at a high resolution with the compositional description is computationally very intensive. Simulating at a lower resolution with a coarse grid reduces the computational loads, but it becomes less accurate. Upscaling procedures are used to convert the high resolution, fine scale simulation parameters to lower resolution, coarse scale simulation parameters.

In this research, an upscaling procedure is examined that uses a thermodynamic non-equilibrium correction to keep a high accuracy for the coarse scale compositional simulation. This non-equilibrium phenomena is represented by a source term in the thermodynamic equilibrium equation. This source term is obtained from a fine scale simulation and upscaling the phase compositions. The source terms are tabulated against the composition and are used in the coarse scale simulation. An isothermal system with $N_c = 3$ number components and $N_p = 2$ number of phases is considered in this research. The capillary and diffusive effects are neglected as well as the chemical reactions and adsorption. For the fine scale, a 2D grid of 102x20 is used and the coarse scale grid is 1D with 102x1 cells. The fine scale simulation is run using Automatic Differentiation General Purpose Research Simulator (AD-GPRS) and the coarse scale simulation is run with an IMPEC simulator written in Matlab.

To quantify the accuracy of the coarse scale simulation a misfit value is calculated between the coarse scale saturation distribution and the upscaled fine scale saturation distribution. Comparing the coarse saturation distribution with the upscaled saturation distribution shows that this method allows high accuracy results to be maintained with non-equilibrium upscaling of the compositional flow.

A correlation is made between the source term and composition and used in a coarse simulation instead of the tables created from the fine scale simulation. This reduces the accuracy compared to the fine scale, but it still gives a satisfactory improvement of coarse scale results. To improve the accuracy of the simulation using the correlation, an optimization procedure is performed. The optimization improved the accuracy to the level of the accuracy of the simulation using the full source term tables. With a correlation between the source term and composition, the global fine scale compositional solution is no longer necessary for the coarse simulation.

Table of Contents

Abstract 5
Table of Contents 6
1 Introduction 7
2 Upscaling procedures 8
2.1 Single-phase upscaling 8
2.1.1 Local upscaling 8
2.1.2 Extended local upscaling 10
2.1.3 Global upscaling 10
2.1.4 Local-global upscaling 11
2.2 Multiphase upscaling 11
2.3 Compositional processes upscaling 13
3 Simulation formulations 15
3.1 Fine scale 16
3.1.1 Negative Flash 16
3.2 Coarse scale 17
3.2.1 Modified Rachford-Rice equation and Negative flash 19
4 Reservoir Description 21
5 Method 23
5.1 Upscaling permeability and transmissibility 23
5.2 Upscaling the relative permeabilities 24
5.3 Upscaling phase compositions and creating source term table 25
5.4 Coarse simulation using source term table 26
5.5 Optimizing source term correlation 26
6 Results 27
6.1 Simulation without thermodynamics 27
6.2 Non-Equilibrium thermodynamic correction 28
6.3 Optimization of source term correlation 33
6.3.1 Optimization 1 33
6.3.2 Optimization 2 36
6.3.3 Optimization 3 39
6.3.4 Optimization 4 41
6.3.5 Optimization 5 44
6.3.6 Optimization 6 45
7 Conclusions and recommendations 48
7.1 Conclusions 48
7.2 Recommendations 49
Bibliography 50
Appendix A Transmissibility conversion factor 53

1 Introduction

As the oil reserves are declining and the “easy to reach and produce” oil fields are no longer available, Enhanced Oil Recovery (EOR) methods are becoming more and more popular in order to increase the recovery factor of a reservoir. One of the most common EOR methods is the injection of miscible gases. For the production of oil and gas, a broadly used tool is reservoir simulation. It can be used for production history matching, performance forecasting and the field development. It is important that the simulation gives an accurate representation of the physics associated with the production of oil or gas, for example when simulating the injection of miscible gases. With the injection of gas the system has to be considered as multiphase and multicomponent. To simulate this type of system, a compositional flow model can be used, which is a more complicated model than for example the black-oil model. Most current upscaling procedures are focused on black-oil models, but the disadvantage of the black-oil model is that it cannot reproduce important compositional effects related to miscible gas injection. Therefore the black-oil model does not give an accurate representation of a multiphase multicomponent system.

Modern EOR processes depend on the heterogeneity of the reservoir. Small scale heterogeneities can be described at a high resolution using modern characterization methods. Using these reservoir properties at a high resolution with a representative physical model for the flow and transport will give an accurate result of the simulation. However, the high resolution together with the more complex compositional flow model makes the simulation computationally very expensive. To cut down on computation times, an upscaling procedure is needed to go from a high resolution fine scale grid to a coarse grid.

In this research, an upscaling procedure for the compositional flow model proposed by Iranshahr, Chen [1] is examined. This upscaling procedure uses the assumption of instantaneous thermodynamic equilibrium on a fine scale, and a thermodynamic non-equilibrium on a coarse scale. The purpose of this research is to investigate the applicability of the non-equilibrium upscaling procedure when using K-values for the vapor-liquid equilibrium calculations. Specifically by adding a source term to the vapor-liquid equilibrium equation to represent the non-equilibrium phenomena and modifying the Rachford-Rice equation. The procedure will be derived and demonstrated for a simple setup with three components.

In this report, the different aspects of upscaling procedures will shortly be explained and followed by the formulations used in the simulation of the reservoir in chapter 2 and 3. For this research, a synthetic reservoir is used which will be described in chapter 4. In chapter 5 the upscaling methods will be described. And finally, the results and conclusions, together with some recommendations for further research, will be shown in chapter 6 and 7.

2 Upscaling procedures

Upscaling is the procedure of substituting a region of fine grid cells with heterogeneous properties with a single coarse grid cell that is homogeneous. In Figure 1, a conceptual illustration of upscaling is shown [2]. To obtain a single coarse scale value of heterogeneous fine scale values, different procedures can be used. Some of these upscaling procedures will be introduced here, more information on the various upscaling methods are explained in Salehi, Tchelepi [3].

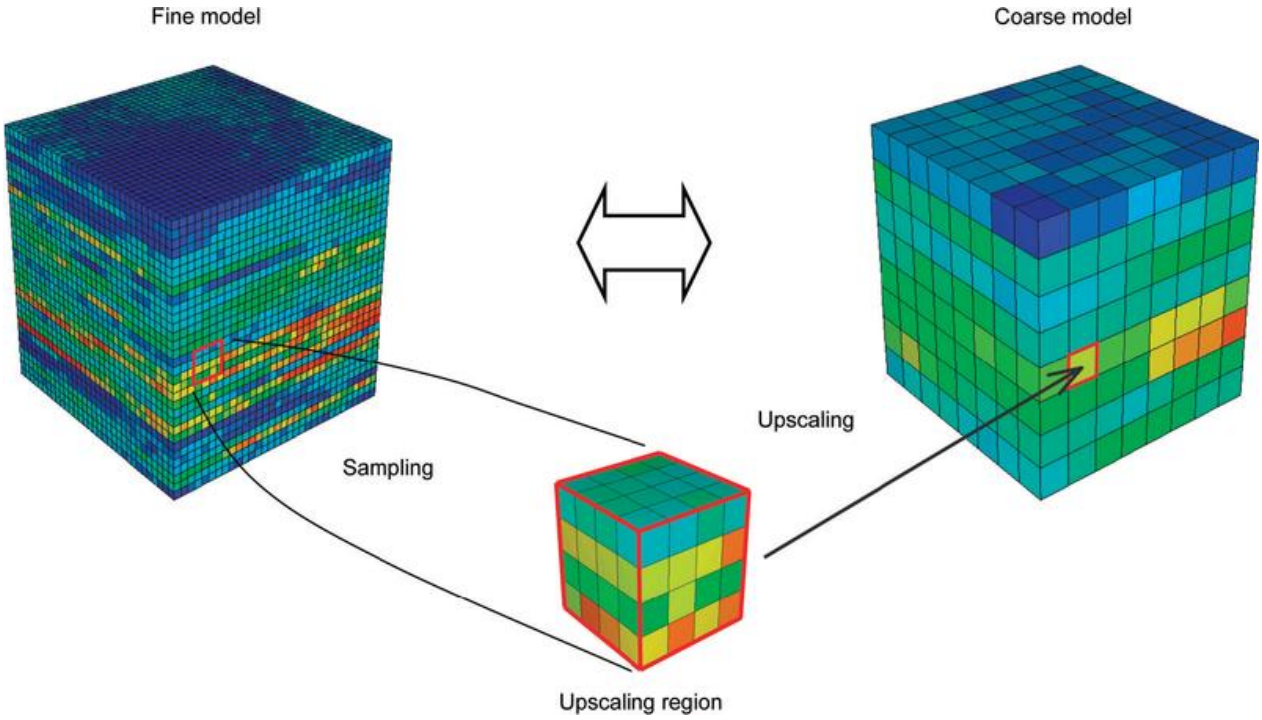

Figure 1 Concept of upscaling heterogeneous fine scale properties. From "PetroWiki", by "Glendasmith", 2013 (http://petrowiki.org/File:Vol5_Page_1423_Image_0001.png)

2.1 Single-phase upscaling

Single-phase upscaling is the upscaling of fine-scale features such as permeability and porosity to predict an equal amount of total single-phase flow through a course block as the summation of the flow through the fine-scale blocks. The upscaled single-phase properties can be used in multiphase or compositional problems. Often single-phase upscaling involves solving the pressure distribution for a single-phase problem over a local or global region of a heterogeneous reservoir. From the known pressure field and single-phase flow rates the upscaled permeabilities or transmissibilities can be calculated. Depending on the size of the region over which the fine scale single-phase simulation is solved, the upscaling procedure is classified as local, extended local, global or local-global.

2.1.1 Local upscaling

An example of a local upscaling procedure is the upscaling of the permeability by solving steady-state, single-phase incompressible flow with no source terms over a region that exactly covers the target coarse block. That region is called the local region. The equation to be solved is given by (2.1).[4]

$$\nabla \cdot \left(\mathbf{k}^f \cdot \nabla p^f \right) = 0 \tag{2.1}$$

With p the dimensionless phase pressure and $\mathbf{k}^f$ the absolute permeability tensor. The superscript f it is a fine scale variable. With upscaled values equation (2.1) becomes (2.2) with $\mathbf{k}^*$ the upscaled permeability tensor and p^c the coarse scale pressure. [4]

$$\nabla \cdot \left(\mathbf{k}^* \cdot \nabla p^c \right) = 0 \tag{2.2}$$

The simplest techniques for calculating the upscaled permeabilities are power averaging procedures introduced by Deutsch [5]. Power averaging does not require any numerical solutions which means they are computationally very efficient. Equation (2.3) gives a basic approach of calculating upscaled permeability using power averaging.

$$k_i^* = \left(\frac{1}{V_{cb}} \int_{V_{cb}} \left(k_i \right)^{\omega_i} dV \right)^{1/\omega_i} \tag{2.3}$$

Here V_{cb} represents the coarse block volume, k_i^* and k_i are considered to be the upscaled and fine scale permeabilities diagonal tensors respectively with i representing the diagonal component. ω_i is the power averaging exponent and can vary with its direction i. The power averaging component is constrained to lie between -1 and 1. The extreme values of this constraint represent layered systems with $\omega = 1$ for flow parallel to the layers and $\omega = -1$ for flow perpendicular to the layers. Using $\omega = 1$ leads to an arithmetic average and $\omega = -1$ to a harmonic average. The geometric mean corresponds to the limit $\omega \to 0$.

When calculating the upscaled permeabilities numerically, equation (2.1) is solved over a local region. The choice of the boundary conditions for this local region are a significant issue in any local or extended local upscaling procedure. The actual conditions imposed on the region during the flow simulation are not known a priori and generally they will vary. This leads to some ambiguity in the choice of the boundary conditions.
An example of possible boundary conditions is shown in Figure 2 [3]. At the left and right side, constant pressure boundary conditions are set to $p = 1$ and $p = 0$ respectively. At the upper and lower sides, a no flow boundary condition is imposed. This setup can be used to calculate the upscaled permeabilities in the x-direction, when calculating the upscaled permeabilities in the y-direction, the boundary conditions are rotated by 90°.[3]

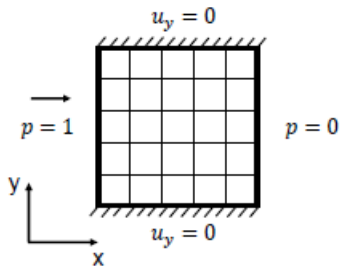

Figure 2 Schematic for local permeability upscaling with constant pressure and no flow boundary conditions. From: Salehi, Tchelepi [3]

Amongst others, Durlofsky [6] applied and analysed periodic boundary conditions. The periodic boundary conditions yield symmetric, positive definite upscaled permeability tensors. Another local treatment is introduced by King and Mansfield [7]. Their procedure imposes linear pressure boundary conditions. It is also possible to obtain the local boundary conditions from the global coarse scale solution, but this is considered as local-global upscaling and will be discussed in section 2.1.2.

The transmissibility can be directly upscaled using the avareging procedures and boundary conditions described above. This eliminates additional approximations needed to calculate the upscaled transmissibility from the upscaled permeability [4]. The transmissibility is defined at the interface between two grid blocks and uses the adjacent grid block permeabilities and geometries. Romeu and Noetinger [8] and Abbaszadeh and Koide [9] reported improved accuracy in their results by using local transmissibility upscaling in comparison to permeability upscaling.

2.1.2 Extended local upscaling

Different authors reported that an improved accuracy for the permeability and transmissibility upscaling can be obtained by solving a larger local problem (Hou and Wu [10] ;Wu, Efendiev [11]). By including the neighbouring regions in the calculation of the permeability or transmissibility, the effects of large scale connectivity or lack thereof can be better captured. A "border region" is added to the local region for which the upscaled permeability or transmissibility is being calculated. This border region consists of a ring of coarse blocks around the target coarse block or interface. This new region that contains the local region and the border region is considered as the extended local region. The size of the extended local region is quantified by the parameter r, which defines the number of rings of coarse cells that are included in the border region. An example of an extended local region is shown in Figure 3, for this region $r=1$.

The same boundary conditions can be applied on this extended local region as for the local region. Because the upscaled permeability is only calculated for a portion of the region, a volume averaging is applied to calculate the upscaled permeability instead of an integration over the boundaries.[4]

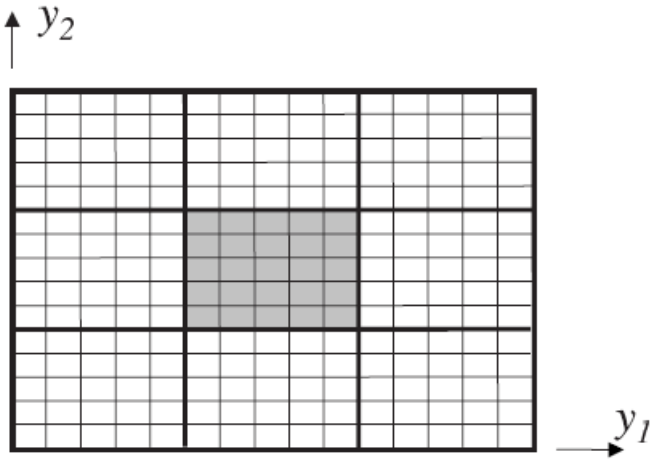

Figure 3 Fine and coarse grids for the target cell in the center and a surrounding border region. From Durlofsky 2005

2.1.3 Global upscaling

The upscaling procedures using local or extended local regions require the specification of (assumed) boundary conditions on the local or extended local region. In global region upscaling procedures the flow problem is solved over the whole reservoir and this solution is used to calculate the upscaled quantities.[4]
White and Horne [12] used fine-scale pressure solutions to compute the coarse scale transmissibilities. To minimize the mismatch in flux between the fine and coarse scale

solutions, they used different boundary conditions and least square regressions. Pickup, Jensen [13] developed a global permeability upscaling procedure based on pressure perturbation. Instead of using arbitrary boundary conditions they use two boundary conditions. The first boundary condition is the actual flow boundary condition and the second boundary condition is the pressure perturbation. A global upscaling procedure based on specific global flow scenarios has been developed by Nielsen and Tveito [14], Holden and Nielsen [15] and Holden, Nielsen [16]. They used optimization techniques to minimize the mismatch in the velocity field between the fine and coarse scale solutions. Zhang, Pickup [17] reported very accurate results for their global transmissibility upscaling procedure for well-driven flow problems. To obtain the global fine scale solution the actual well settings were used. Chen, Mallison [18] and Chen and Li [19] applied iteration to increase the accuracy of the upscaled functions for their proposed upscaling procedures.

Global upscaling procedures are very accurate, but they are also computationally expensive since the global fine scale solutions are needed. The high computational cost of the global upscaling procedure for the transmissibility can often be justified by the fact that the upscaled transmissibility can be used for multiphase flow problems without the need to upscale the relative permeability functions. The combination of accurate single-phase properties with fine scale relative permeability function often provide sufficient accuracy if the upscaling ratio is not too high.[17]

2.1.4 Local-global upscaling

Local-global approach is, as the name suggests, a combination of local and global upscaling. It is a method that estimates the effects of the global flow problem without solving the global fine-scale problem. The advantage of local global upscaling that it tries to maintain the high accuracy of global upscaling but keeping the computational costs low. Chen, Durlofsky [20] use global coarse scale simulations to estimate the boundary conditions for a local or extended local upscaling. An iteration procedure is used to assure consistency between the local and global calculations. This procedure is shown to give more accurate results for highly heterogeneous systems compared to existing local or extended local upscaling procedures. Chen and Durlofsky [21] [22] and Chen and Li [23] applied the local global approach to well-driven flow scenarios and three-dimensional problems. Chen and Li [23] also extended the local global upscaling procedure for multiphase flow problems.

2.2 Multiphase upscaling

Single-phase upscaling only considers the singe-phase pressure equation. For multiphase flow, the transport equations need to be considered. Although single-phase upscaling can give satisfactory results for some multiphase cases, it does not consider the parameters in the transport equations and thus leads to an inaccuracy. An example of a transport equation parameter is the relative permeability. The upscaling errors become more pronounced in cases with high mobility ratio displacements and/or large upscaling ratios. To remedy this, multiphase upscaling procedures are needed that can upscale the transport equation parameters such as the relative permeability.[3]

In an attempt to capture the effects of heterogeneities not represented on the coarse simulation grid of multiphase fluid flow, dynamic pseudo-relative permeability functions are often used. Dynamic means that the pseudo-relative permeability functions are generated from a fine-scale simulation model.[3] Some severe difficulties common to all dynamic pseudo-relative permeability methods are: choosing the number and locations of the coarse grid rock types,

defining simulations from which the pseudos' are generated, and the dependence of the pseudos' on well rates and positions. Barker and Thibeau [24] concluded that pseudo-relative permeability functions cannot be used reliably to scale up from a "fine-grid" geological model to a "coarse-grid" fluid flow model except for cases where the capillary and gravity effects are on the coarse grid block scale. Barker and Dupouy [25] analyzed six widely used dynamic pseudo-relative permeability methods for the case of incompressible, immiscible and two-phase flow. Additional analyses of dynamic pseudo-relative permeability methods was done by Darman, Pickup [26]. They focused on the methods based on fluid potential. Durlofsky and Chen [27] made a comparison between some of the existing two-phase upscaling procedures as well.

The two main methods for multiphase upscaling are Kyte and Berry [28] and Stone [29]. Many subsequent methods can be categorized as their extensions [3]. Kyte and Berry [28] use the Darcy equation for multiphase flow and assume upstream permeability weighting in their calculation of the dynamic pseudo-relative permeabilities. The densities and viscosities are evaluated at the arithmetic average pressure. Stone [29] used the total mobility and fractional flow functions as the upscaled functions. For obtaining the transmissibility, the weighted average of the fine scale mobilities is calculated along the coarse interfaces. The difference between the potential in different phases is ignored in Stone's method. However, these potential differences occur for cases with strong gravity effects [26]. The method of Stone does avoid some of the drawbacks associated with estimating the average pressure in the method from Kyte and Berry.

An important aspect in upscaling of multiphase flow properties is the domain over which the upscaled functions are calculated. Because of the high computational costs associated with global fine scale multiphase simulations, these are preferably avoided. Using smaller local regions for the multiphase upscaling procedures has the impact of the choice of boundary conditions as drawback. In addition to the pressure boundary conditions needed for single-phase upscaling, saturation boundary conditions are required as well. A set of standard boundary conditions for multiphase upscaling of a local region is shown in Figure 4[3].

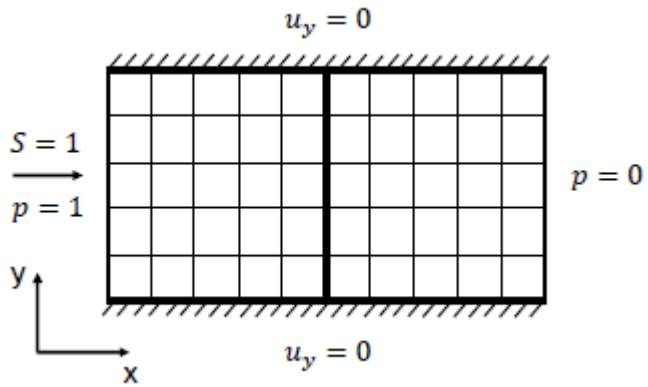

Figure 4 Generic boundary conditions for the pressure and saturation for upscaling of multiphase flow problems. From: Salehi, Tchelepi [3]

Chen and Durlofsky [21] and Chen and Li [23] have shown that these standard boundary conditions can overestimate the injected fluid flow and predict an earlier breakthrough for highly heterogeneous permeability fields. This issue is addressed by Wallstrom et. al. in [30] and [31] with the effective flux boundary conditions(EFBC). Local fine scale permeability and global background permeability are used in these methods to estimate the local flux boundary conditions. Applying the EFBC methods for relative permeability upscaling

calculations are reported by Hui and Durlofsky [32] and Chen and Durlofsky [21] to yield more accurate results compared to methods using standard boundary conditions.

2.3 Compositional processes upscaling

For systems with miscible or near-miscible gas injection, and oil vaporization due to lean gas injection it is necessary to perform a compositional simulation for an accurate result. Variations in phase saturations and compositions occur on a fine scale for processes such as miscible or near-miscible gas injection. These variations are driven by viscous fingering, reservoir heterogeneity and the development of narrow fronts across which phase compositions change rapidly [33].

Because it is computationally expensive applying compositional simulation using a high resolution, an upscaling procedure is needed that gives an accurate coarse scale representation. Because most existing upscaling techniques focus on black-oil and multiphase models, there is no established procedure to compensate for the failure to resolve fine scale variations when using compositional simulation with an equation of state when using larger grid blocks. For black-oil simulation effective permeabilities and pseudo relative permeability functions can be used to improve the results. In compositional simulation with a coarse grid there are three categories of errors: numerical dispersion, improper averaging of the effects of the subscale heterogeneities, and inaccurate phase behavior calculations [34, 35]. Some of the work done on the upscaling for compositional flow problems will be discussed below. Camy and Emanuel [36] used pseudo relative permeability curves and pseudo K-values to reduce the grid size sensitivity in compositional simulation.

To represent the averaging effect of the fine scale heterogeneities in an Equation of State compositional model, Fayers, Barker [34] proposed a Dual Zone Mixing (DZM) procedure. In this procedure each coarse grid block is split into a contacted and a bypassed zone. For each of the zones a separate phase behavior calculation is made to model the nonuniform phase behavior over the coarse grid block. A similar approach was developed by Evazi and Jessen [37] and Zhang and Okuno [38]. They arranged the porosity into two levels of porosity based on the flow contribution. For the coarse scale flow simulation a dual-porosity dual-permeability flow model is adapted. It must be noted that the dual-porosity model could be too time consuming for application on a field-scale [39].

Barker and Fayers [35] introduced transport coefficients (α-factors) in the flow terms of a compositional simulator. The α-factors model the interaction between phase behavior and reservoir heterogeneity within the coarse grid blocks. The α-factors are obtained from the component fluxes through the coarse scale interfaces. Barker and Fayers used their method successfully to model lean and rich gas injection in stochastically-generated, heterogeneous reservoir cross-sections and their method is used in commercial simulators. Christie and Clifford [40] used a streamline technique to produce upscaled fluxes. The streamline technique provides a speed gain for the calculation with a small loss of accuracy. Their obtained upscaled fluxes are almost identical to those obtained from conventional compositional simulations. The upscaled fluxes can be used to obtain the α-factors.

For compositional simulation, an instantaneous thermodynamic phase equilibrium is assumed in each grid block. Thereby, the phase behavior calculation is based on a complete mixing of all components. On small scales, this assumption is valid with diffusive effects ensuring a good mixing on this scale. However, variations in fluid compositions on scales smaller than

the typical grid block size are caused by sub-grid heterogeneities. Nghiem and Sammon [41] described an equation of state compositional simulator where the oil and gas approach a thermodynamic equilibrium through a rate process. The thermodynamic equilibrium is only instant at the interface between the oil and gas phases and a diffusion process drives the oil and gas compositions towards this equilibrium. A new upscaling procedure based on non-equilibrium thermodynamic concept is proposed by Iranshahr, Chen [1]. Instantaneous thermodynamic equilibrium is assumed for the fine scale, but a non-equilibrium term is introduced to the thermodynamic constraints on the coarse scale. More precisely, a source term is added to the upscaled fugacity equality. The fine scale simulation results are used to upscale the fugacity functions and to calculate the source term.

Salehi, Tchelepi [3] extended this approach and introduced a physical non-equilbrium source term for local thermodynamic constraints. They demonstrated that the resulting tie-lines in the coarse scale are tilted compared to the equilibrium tie-lines. A method for the conversion of the non-equilibrium thermodynamic functions into the transport equations (α-factors) is described as well. Based on the tilted tie-lines, Salehi, Tchelepi [3] introduced a calculation of modified K-values for the coarse simulation. The coarse scale K-values are calculated from the upscaled phase compositions.

For this research the non-equilibrium term will be added to the coarse scale thermodynamic constraints. This is done in the form of a source term in the thermodynamic equilibrium equation instead of modifying the K-values for the coarse scale. This approach leads to a modified Rachford-Rice equation. The source term is obtained with the upscaled phase compositions. This source term is tabulated against the composition and this table is used in the coarse scale simulation. An attempt is made to find a correlation between the source term and composition from the source term tables. To improve this correlation, an optimization procedure is executed. With a correlation between the source term and composition, the global fine scale compositional solution is no longer necessary for the coarse simulation.

3 Simulation formulations

For this research, an isothermal system with $N_c = 3$ number of components and $N_p = 2$ number of phases is considered. The capillary and diffusive effects are neglected as well as the chemical reactions and rock adsorption.
As described by Salehi, Voskov [42], the equations used in the simulations are shown here below. For the fine scale the system is solved with the Automatic Differentiation General Purpose Research Simulator (AD-GPRS) [43]. The coarse scale simulation is written in Matlab and is an Implicit Pressure Explicit Composition (IMPEC) simulator. The equations for the IMPEC simulator will be shown in section 3.2.

The mass conservation equation for component x_i is given by (3.1).

$$\frac{\partial}{\partial t}\left(\phi\sum_{j=1}^{N_P} x_{ij}\rho_j S_j\right) - \nabla\cdot\left(\sum_{j=1}^{N_P} x_{ij}\rho_j u_j\right) + \sum_{j=1}^{N_P} x_{ij}\rho_j q_j = 0, \quad i = 1,\ldots,N_C \tag{3.1}$$

Where ϕ is the porosity, t is time, x_{ij} the mole fraction of component i in phase j, u_j is the Darcy velocity of phase j and q_j is the production term for phase j.

Using Darcy's law the Darcy velocity u_j can be calculated with equation (3.2),

$$u_j = -\mathbf{k}\lambda_j\cdot\left(\nabla p - \gamma_j\nabla D\right) \tag{3.2}$$

where $\mathbf{k}$ is the absolute permeability, $\lambda_j = \frac{k_{rj}}{\mu_j}$ the phase mobility with k_{rj} the relative permeability and μ_j the viscosity of phase j. The pressure p is the same for all phases when the capillary effects are neglected. In equation (3.2), γ_j is the vertical pressure gradient and D is the depth which is assumed positive in the downward direction.
Combining equations (3.1) and (3.2) the mass conservation equation will be as given in (3.3).

$$\frac{\partial}{\partial t}\left(\phi\sum_{j=1}^{N_P} x_{ij}\rho_j S_j\right) - \nabla\cdot\left(\sum_{j=1}^{N_P} x_{ij}\rho_j\lambda_j\mathbf{k}\cdot\nabla p\right) + \sum_{j=1}^{N_P} x_{ij}\rho_j q_j = 0, \quad i = 1,\ldots,N_C \tag{3.3}$$

When standard finite volume discretization is applied on equation (3.3) for a rectangular structured grid equation (3.4) is obtained.

$$\frac{\partial}{\partial t}V\left[\phi\left(\sum_{j=1}^{N_P} x_{ij}\rho_j S_j\right)\right] - \sum_l\left(\sum_{j=1}^{N_P} x_{ij}^l\rho_j^l\lambda_j^l T^l\Delta p^l\right) + \sum_{j=1}^{N_P} x_{ij}\rho_j Q_j = 0, \quad i = 1,\ldots,N_C \tag{3.4}$$

Here V is the cell volume, T the transmissibility and l represents the interfaces between grid blocks. The superscript l means the variables are defined at the interface. To solve this system additional constraints are needed. Two simple ones are that of the mole fractions of the component in each phase and the phase saturation as shown in (3.5) and (3.6).

$$\sum_{i=1}^{N_C} x_{ij} = 1, \quad j = 1,\ldots,N_p \tag{3.5}$$

$$\sum_{j=1}^{N_P} S_j = 1 \tag{3.6}$$

The thermodynamic constraint will be different for the fine scale simulation and the coarse scale simulation.

3.1 Fine scale

For the fine scale simulation the composition calculations are based on vapor-liquid equilibrium equation as shown in (3.7).

$$y_i = K_i \cdot x_i \tag{3.7}$$

The K-values are given and this is then used in the negative flash procedure to calculate the phase compositions. The negative flash procedure will be explained below.

3.1.1 Negative Flash

To determine the phase compositions, a calculation of the vapor-liquid equilibrium is performed. For this calculation, the negative flash procedure is used as described by Whitson and L. Michelsen [44]. This is called the negative flash procedure because it is possible to obtain a negative phase saturation. A negative saturation is a non-physical solution, but it means the composition is in a single-phase state. This means the procedure can give a solution regardless of the state.
The total composition, the pressure and the temperature are known. The component material balance given by (3.8) has to be satisfied.

$$z_i \cdot n = y_i \cdot n_V + x_i \cdot n_L \tag{3.8}$$

When introducing the vapor mole fraction β as (3.9), equation (3.8) can be rewritten as (3.10).

$$\beta = \frac{n_V}{n} \tag{3.9}$$

$$z_i = y_i \cdot \beta + x_i \cdot (1-\beta) \tag{3.10}$$

The mole fractions of the different phases, x_i and y_i, must also sum to 1 when in equilibrium.

$$\sum_{i=1}^{N} x_i = \sum_{i=1}^{N} y_i = 1 \tag{3.11}$$

To solve for y_i, x_i and β the Rachford-Rice equation (3.12) is used. The Rachford-Rice equation is based on combining equations (3.7) and (3.10) and constraint (3.11).

$$h(\beta) = \sum_{i=1}^{N} y_i - \sum_{i=1}^{N} x_i = \sum_{i=1}^{N} (y_i - x_i) = \sum_{i=1}^{N} \frac{z_i \cdot (K_i - 1)}{1 + \beta \cdot (K_i - 1)} = 0 \tag{3.12}$$

For the function (3.12), singularities occur at $\beta = \frac{1}{(1-K_i)}$ and has solutions between all the asymptotes. However, only the solution between the asymptotes given by (3.13) yields all non-negative phase compositions y_i and x_i.

$$\begin{aligned} \beta_{\min} &= \frac{1}{(1-K_{\max})} \\ \beta_{\max} &= \frac{1}{(1-K_{\min})} \end{aligned} \tag{3.13}$$

The function (3.12) is solved using the bisection method between the two boundaries for β given in (3.13). After the correct β has been calculated within an acceptable tolerance the phase compositions can be calculated with equations (3.14) and (3.15).

$$x_i = \frac{z_i}{1+\beta\cdot(K_i-1)} \tag{3.14}$$

$$y_i = \frac{z_i\cdot K_i}{1+\beta\cdot(K_i-1)} = x_i\cdot K_i \tag{3.15}$$

3.2 Coarse scale

For the fine scale an instantaneous equilibrium between the two-phases is assumed and represented by the vapor-liquid equilibrium equation (3.7). For the coarse scale a source term is added to this vapor-liquid equilibrium equation to represent the non-equilibrium. This will be discussed in more detail in section 3.2.1. First the IMPEC simulation will be discussed.

For the coarse scale the simulation is based on implicit pressure calculation and an explicit compositional calculation, IMPEC. Implicit means the calculation is performed using current time values of the variables in all grid blocks. Explicit means the previous time values of variables are used to calculate a current time value.
At time step t, first the new composition Z_t is calculated. This is done using equation (3.22). Since this is incompressible flow the velocity is constant as given in (3.16).

$$U_t = -k\left(\frac{k_{ro}}{\mu_o}+\frac{k_{rg}}{\mu_g}\right)\nabla p = const \tag{3.16}$$

Next, the fractional flow function for the gas phase is introduced:

$$f = \frac{k_{rg}}{\mu_g}\Bigg/\left(\frac{k_{rg}}{\mu_g}+\frac{k_{ro}}{\mu_o}\right) \tag{3.17}$$

The velocities can be written using the fractional flow term from (3.17) as shown in (3.18).

$$\begin{aligned} U_g &= -k\frac{k_{rg}}{\mu_g}\nabla p = f\cdot U_t \\ U_o &= (1-f)U_t \end{aligned} \tag{3.18}$$

The compositional fractional flow can then be written as (3.19) for component i.

$$F_i = y_i f + x_i(1-f) \tag{3.19}$$

With V as the vapor fraction the overall composition can be written as (3.20).

$$Z_i = y_i V + x_i(1-V) \tag{3.20}$$

Conservation equation in terms of fractional flow is given by (3.21).

$$\frac{\partial Z_{\mathrm{i,n,t}}}{\partial t}+\frac{U_{n,t}}{\phi}\frac{\partial F_{i,n,t}}{\partial x} = 0 \tag{3.21}$$

Discretizing equation (3.21) leads to equation (3.22) which is used to calculate the new composition Z_t.

$$Z_{i,n,t} = Z_{i,\mathrm{n},t-1} - \frac{U_{i,n} \cdot \Delta t}{\phi \cdot \Delta x} \cdot \left(F_{i,n,t-1} - F_{i,n-1,t-1} \right) \tag{3.22}$$

Here $F_{i,t}$ is the fractional flow and $U_{i,t}$ the Darcy velocity in grid block n at time step t. With the composition known the negative flash procedure can be used to calculate the phase compositions and phase saturations.

The next step is to determine the relative permeabilities with the lookup tables generated from the fine scale simulation. These relative permeabilities are used for the pressure calculation. The equation used to calculate the pressure is derived from the mass balance equation (3.23) of component x_i.

$$\frac{\partial}{\partial t}\left(\phi \sum_{j=1}^{N_P} x_{ij} \rho_j S_j \right) - \nabla \cdot \left(\sum_{j=1}^{N_P} x_{ij} \rho_j u_j \right) + \sum_{j=1}^{N_P} x_{ij} \rho_j q_j = 0, \quad i = 1, \ldots, N_C \tag{3.23}$$

The densities are set to be equal for all phases and compressibility is neglected in this research the density can be divided out of the equation. The coarse scale flow is in one dimension in the x-direction. With this the balance equation can be written as (3.24).

$$\phi \frac{\partial}{\partial t}\left(\sum_{j=1}^{N_P} x_{ij} S_j \right) + \frac{\partial}{\partial x} \cdot \left(\sum_{j=1}^{N_P} x_{ij} u_j \right) + \sum_{j=1}^{N_P} x_{ij} q_j = 0, \quad i = 1, \ldots, N_C \tag{3.24}$$

With the Darcy equation and the mobility defined as (3.25) and (3.26) respectively and using $Z_i = \sum_{j=1}^{N_P} x_{ij} S_j$, the balance equation can be rewritten as (3.27).

$$u_j = -\mathbf{k} \cdot \frac{k_{rj}}{\mu_j} \cdot \frac{\partial p}{\partial x} \tag{3.25}$$

$$\lambda_j = \frac{\mathbf{k} \cdot k_{rj}}{\mu_j} \tag{3.26}$$

$$\phi \frac{\partial Z_i}{\partial t} - \frac{\partial}{\partial x} \cdot \left(\sum_{j=1}^{N_P} x_{ij} \lambda_j \frac{\partial p}{\partial x} \right) + \sum_{j=1}^{N_P} x_{ij} q_j = 0, \quad i = 1, \ldots, N_C \tag{3.27}$$

Now summing over all components gives equation (3.28).

$$\phi \frac{\partial}{\partial t}\left(\sum_{i=1}^{N_c} Z_i \right) - \frac{\partial}{\partial x} \cdot \left(\sum_{i=1}^{N_c} \sum_{j=1}^{N_P} x_{ij} \lambda_j \frac{\partial p}{\partial x} \right) + \sum_{i=1}^{N_c} \sum_{j=1}^{N_P} x_{ij} q_j = 0 \tag{3.28}$$

The summation over the composition is always $\sum_{i=1}^{N_c} Z_i = 1$ so $\frac{\partial}{\partial t}\left(\sum_{i=1}^{N_c} Z_i \right) = 0$. The summation of phase composition will also always result in $\sum_{i=1}^{N_c} x_{ij} = 1$ with j the phase. This leaves us with equation (3.29) from which the pressure can be solved.

$$-\frac{\partial}{\partial x}\left(\lambda_{tot}\frac{\partial p}{\partial x}\right)+q_{tot}=0 \tag{3.29}$$

With $\lambda_{tot}=\sum_{j=1}^{N_p}\lambda_j$ and $q_{tot}=\sum_{j=1}^{N_p}q_j$. This equation can be discretized and solved numerically to obtain the pressure distribution. For the discretization equation (3.30) is used. Here i represents the grid center and $i+\frac{1}{2}$ represent the interface location between grid block i and $i+1$. All grid blocks are of equal size so Δx does not change.

$$-\frac{\partial}{\partial x}\left(\lambda_{tot}\frac{\partial p}{\partial x}\right)\approx-\left(\frac{\lambda_{tot,i+\frac{1}{2}}}{\Delta x}\left(\frac{\Delta p}{\Delta x}\right)_{i+\frac{1}{2}}-\frac{\lambda_{tot,i-\frac{1}{2}}}{\Delta x}\left(\frac{\Delta p}{\Delta x}\right)_{i-\frac{1}{2}}\right) \tag{3.30}$$

The interface mobility $\lambda_{tot,i+\frac{1}{2}}$ is calculated using the harmonic average of $\lambda_{tot,i}$ and $\lambda_{tot,i+1}$. Discretizing further gives equation (3.31).

$$-\left(\frac{\lambda_{tot,i+\frac{1}{2}}}{\Delta x}\left(\frac{p_{i+1}-p_i}{\Delta x}\right)-\frac{\lambda_{tot,i-\frac{1}{2}}}{\Delta x}\left(\frac{p_i-p_{i-1}}{\Delta x}\right)\right)+q_{tot}=0 \tag{3.31}$$

This can be rewritten as equations (3.32) and (3.33).

$$\left(\lambda_{tot,i+\frac{1}{2}}-\lambda_{tot,i-\frac{1}{2}}\right)\frac{p_i}{\Delta x^2}-\lambda_{tot,i+\frac{1}{2}}\frac{p_{i+1}}{\Delta x^2}-\lambda_{tot,i-\frac{1}{2}}\frac{p_{i-1}}{\Delta x^2}+q_{tot}=0 \tag{3.32}$$

$$p_i=\frac{\lambda_{tot,i+\frac{1}{2}}}{\left(\lambda_{tot,i+\frac{1}{2}}-\lambda_{tot,i-\frac{1}{2}}\right)}p_{i+1}+\frac{\lambda_{tot,i-\frac{1}{2}}}{\left(\lambda_{tot,i+\frac{1}{2}}-\lambda_{tot,i-\frac{1}{2}}\right)}p_{i-1}-q_{tot}\Delta x^2 \tag{3.33}$$

3.2.1 Modified Rachford-Rice equation and Negative flash

To account for the non-equilibrium in the coarse scale, a source term is added to the vapor-liquid equilibrium equation. Now the vapor-liquid equilibrium is used as shown by (3.34).

$$y_i=K_i\cdot x_i+\Delta f_i \tag{3.34}$$

The addition of the source term has consequences to the equations used for the negative flash procedure. The Rachford-Rice equation is used to determine the vapor fraction, but this equation has to be reconstructed now taking the source term in account.

$$z_i=(1-\beta)\cdot x_i+\beta\cdot y_i \tag{3.35}$$

Writing (3.35) with z_i as just a function of β and x_i and y_i gives the equations in (3.36).

$$\begin{aligned} z_i&=(1-\beta)\cdot x_i+\beta\left(K_i\cdot x_i+\Delta f_i\right)\\ z_i&=(1-\beta)\cdot\frac{y_i-\Delta f_i}{K_i}+\beta\cdot y_i \end{aligned} \tag{3.36}$$

Rewriting as a function for x_i and y_i gives (3.37).

$$x_i = \frac{z_i - \beta \cdot \Delta f_i}{1 - \beta + \beta \cdot K_i}$$
$$y_i = \frac{z_i \cdot K_i + (1 - \beta) \cdot \Delta f_i}{1 - \beta + \beta \cdot K_i} \tag{3.37}$$

Now using the restriction on x_i and y_i given by (3.11) equation (3.38) holds.

$$\sum x_i - \sum y_i = 0 \tag{3.38}$$

Filling x_i and y_i from (3.37) into (3.38) gives (3.39).

$$\sum \frac{z_i - \beta \cdot \Delta f_i}{1 - \beta + \beta \cdot K_i} - \sum \frac{z_i \cdot K_i + (1 - \beta) \cdot \Delta f_i}{1 - \beta + \beta \cdot K_i} = 0 \tag{3.39}$$

This leads to the new Rachford-Rice equation given by (3.40).

$$\sum \frac{(1 - K_i) \cdot z_i - \Delta f_i}{1 - \beta + \beta \cdot K_i} = 0 \tag{3.40}$$

This function will be used with the bisection method to find β. Once β is known the compositions x_i and y_i can be calculated using (3.37).

4 Reservoir Description

To test the upscaling procedures, a synthetic test case is introduced. A rectangular reservoir with a length of 816 meters, a width of 80 meters and a height of 5 meters is considered for this. The depth of the reservoir is 1000 meters beneath the surface. The porosity and temperature are set constant at 30% and 350 K respectively. The initial pressure in the reservoir is 70 Bar. The injection is set in the cells at the left boundary of the reservoir and the production is set from the cells at the right side. The permeability of the reservoir is defined in a grid of 102x20x1 blocks of equal size. This creates grid blocks of 8x4x5 meters. The 102x20x1 grid is considered to be the fine scale grid in the simulation. The grid of the reservoir is depicted schematically in Figure 5 with Nx=102, Ny =20 and Nz=1. The blue cells represent the injection well and the red cells represent the production well. Because the number of cells in the z-direction is one, this is a 2D problem. The injection pressure at the injection well is set to 100 bars and the production pressure is set to 40 bars.

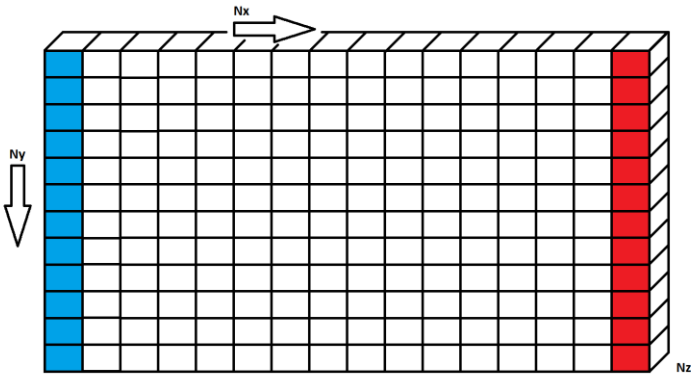

Figure 5 schematic view of the fine scale grid

The fine scale grid upscaled to a coarse grid of 102x1x1 cells. The coarse grid is depicted schematically in Figure 6. Because of the reduction of cells in y-direction this becomes a 1D problem.

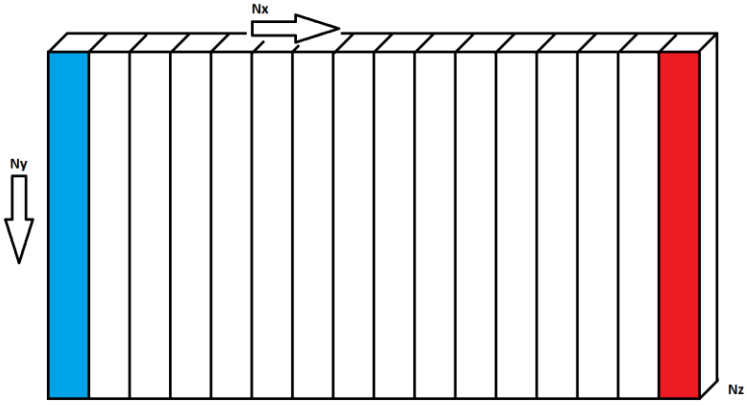

Figure 6 schematic view of the coarse scale grid of the reservoir.

For this research, two different reservoirs with the same size and fine scale grid are created. This is done by using two different permeability distributions with the fine scale grid.
The first permeability distribution is depicted in Figure 7 with the permeability in milliDarcy.

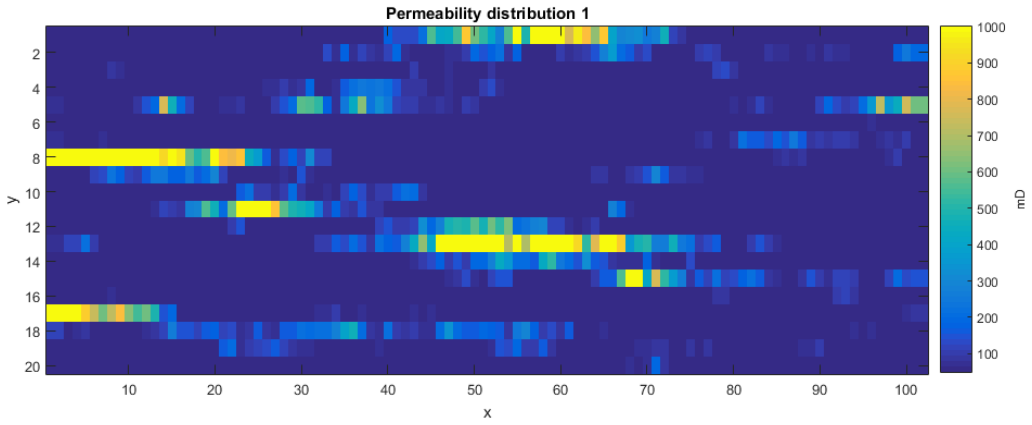

Figure 7 Permeability distribution 1 in mD for the fine scale grid of the reservoir

A second permeability field was created to see if the upscaling method works for a different saturation distribution. For the second case, the reservoir is split in two vertical regions with a permeability distribution with different correlation lengths. This division can clearly be seen in Figure 8. The left side has correlation lengths of $L_{cx1} = 0.8m$ and $L_{cy1} = 0.4\text{m}$ in the x and y direction respectively. On the right side the correlation lengths are increase to $L_{cx2} = 2.4m$ and $L_{cx2} = 1.6m$ in the x and y direction respectively.

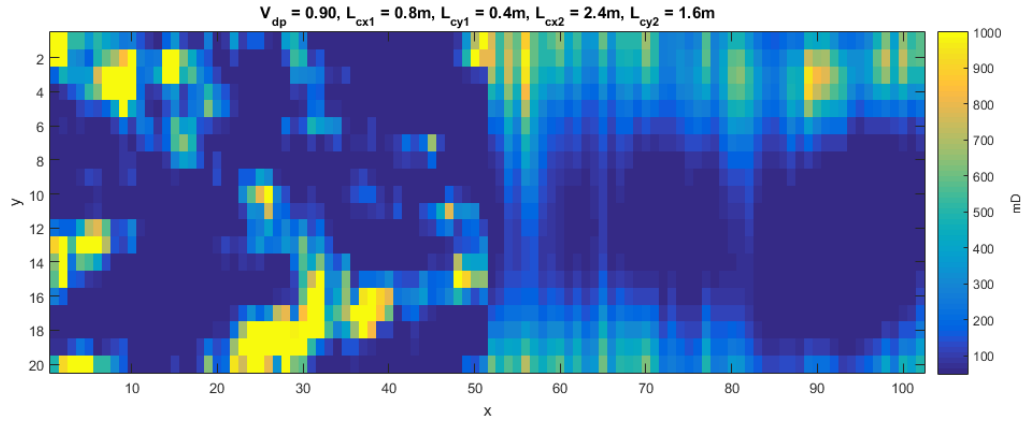

Figure 8 Permeability distribution 2 in mD for the fine scale grid of the reservoir

5 Method

After introducing the reservoir, the simulation can be performed. First the fine scale simulation is run using the Automatic Differentiation General Purpose Research Simulator (AD-GPRS) [43]. The fine scale simulation gives various output variables such as the gas saturation, phase composition, pressure and density in each fine scale grid block. These variables can be used for the upscaling procedures. The saturations and compositions can be used to compare the coarse scale results with the fine scale result by upscaling the values. The different upscaling methods applied in this research are shown in this chapter.

The coarse simulation is run using an IMPEC simulator written in Matlab. This simulator uses upscaled values from the fine scale simulation. Both the fine scale and coarse scale simulation, simulate the transport through the reservoir for a period of 500 days.

5.1 Upscaling permeability and transmissibility

For the upscaling of the permeability and transmissibility any single-phase method can be used [1]. In this case the upscaled permeabilities are obtained from a single-phase simulation over the fine scale permeabilities. From this fine scale simulation the pressure and volume flow are upscaled over the coarse block as shown in equations (5.1) and (5.2). This is a global single-phase upscaling method.

$$q^* = \sum_{b_c} q \tag{5.1}$$

$$p^* = \frac{\sum_{b_c} p}{b_c} \tag{5.2}$$

$$k^* = \frac{q^* \cdot \Delta x_c}{p^* \cdot \Delta z_c \cdot \Delta y_c} \tag{5.3}$$

The upscaled permeability is then calculated using equation (5.3). The superscript * indicates the upscaled value. Because the volume flow is a value at the interface between two grid blocks, the permeability calculated with (5.3) is also a value for the interface. However, permeability should be a property of a grid block and not the interface between two grid blocks. The interface values are considered to be a harmonic average of the grid center values, using this the values from the grid centers can be obtained. In (5.4) an example of this is shown with $\bar{X}_n$ the harmonic average at the interface between two values x_n and x_{n+1} both defined in the grid centers.

$$\begin{aligned} \bar{X}_n &= \frac{2}{\frac{1}{x_n} + \frac{1}{x_{n+1}}} \\ \frac{1}{x_{n+1}} &= \frac{2}{\bar{X}_n} - \frac{1}{x_n} \\ x_{n+1} &= \frac{1}{\frac{2}{\bar{X}_n} - \frac{1}{x_n}} \end{aligned} \tag{5.4}$$

When following (5.4), it is not possible to solve for x_{n+1} with only knowing the value of $\bar{X}_n$, one value of x_n needs to be known as well. This is solved by defining the value x of grid blocks 1 and 2 equal. This results in (5.5) to find the value of x_1 with just $\bar{X}_1$ known.

$$\begin{aligned} \bar{X}_1 &= \frac{2}{\frac{1}{x_1}+\frac{1}{x_2}} \\ x_1 &= x_2 \\ \bar{X}_1 &= \frac{2}{\frac{2}{x_1}} = x_1 \end{aligned} \tag{5.5}$$

These steps are used to calculate the permeabilities in the grid centers from the interface values. The transmissibility at the interface of two grid blocks can be calculated from the permeabilities at the interface and size of the grid blocks. The transmissibility in the x-direction and y-direction is given by (5.6).

$$T_x = k_x \cdot \frac{\Delta Y \cdot \Delta Z}{\Delta X},\ T_y = k_y \cdot \frac{\Delta X \cdot \Delta Z}{\Delta Y} \tag{5.6}$$

With k_x the permeability at the interface and ΔX the distance between the two centers of the grid blocks. Because the units for the permeability and the transmissibility used in the simulation are different, a factor has to be introduced to account for the unit conversion.

$$T_x = k_x \cdot \frac{\Delta Y \cdot \Delta Z}{\Delta X} \cdot C_T \tag{5.7}$$

In Appendix A an analysis on the units is done and the conversion factor C_T is calculated.

5.2 Upscaling the relative permeabilities

Because this is a multiphase system the relative permeabilities need to be upscaled as well. The upscaled relative permeabilities are calculated from the upscaled molar mobilities. Upscaling the pressure and density is done using equations (5.8) and (5.9) with n_{bc} the number of fine blocks in the coarse block.

$$\bar{p} = \frac{\sum_i^{n_{bc}} p_i}{n_{bc}} \tag{5.8}$$

$$\bar{\rho} = \frac{\sum_i^{n_{bc}} \rho_i}{n_{bc}} \tag{5.9}$$

This is simply taking the average pressure and density of the fine scale values inside the coarse block since the volumes of all fine scale blocks are equal.

From Darcy's law and using the mobility defined as $\lambda_j = \frac{k_{r,j}}{\mu_j}$, the steps in (5.10) are derived.

$$q_j = \frac{\kappa_j \cdot A}{\mu_j}\frac{\partial p}{\partial x} = k \cdot \frac{k_{r,j}}{\mu_j} \cdot A \cdot \frac{\partial p}{\partial x} = k \cdot \lambda_j \cdot A \cdot \frac{\partial p}{\partial x} \tag{5.10}$$

The simulation is not performed with infinitesimal volumes so $\frac{\partial p}{\partial x}$ is replaced with $\frac{\Delta p}{\Delta x}$.

When the transmissibility is defined as $T_x = \frac{k \cdot A}{\Delta x}$ the equation for the volume flow of phase j becomes:

$$q_j = \lambda_j \cdot T_x \cdot \Delta p \tag{5.11}$$

Upscaling the mass flow is done by summation of the mass flow through the fine scale blocks in the coarse block. This is shown by equation (5.12).

$$\overline{\rho_j \cdot q_j} = \sum_{B_c} \left(\rho_j \cdot \lambda_j \cdot T \cdot \Delta p \right) \tag{5.12}$$

The steps taken to obtain the upscaled relative permeabilities are shown below:

$$\left(\rho_j \cdot \lambda_j \right)_x^* \cdot T_x^* = \frac{\overline{\rho_j \cdot q_j}}{\Delta \overline{p}} \tag{5.13}$$

$$\lambda_{j,x}^* = \frac{\overline{\rho_j \cdot q_j}}{\Delta \overline{p}} \cdot \frac{1}{T_x^* \cdot \overline{\rho_j}} \tag{5.14}$$

$$\lambda_j^* = \frac{k_{r,j}^*}{\mu_j} \tag{5.15}$$

$$k_{r,j}^* = \lambda_j^* \cdot \mu_j \tag{5.16}$$

These upscaled relative permeabilities are tabulated against the saturation in the coarse block at that time step. This results in relative permeability curves that are used for the coarse scale simulation. This upscaling procedure is multiphase global upscaling, this means we need the full fine scale simulation results for this upscaling procedure.

5.3 Upscaling phase compositions and creating source term table

For the upscaling of the composition, the status (single-phase oil, single-phase gas or two-phase) of the grid block needs to be considered. In equation (5.17) the upscaling for the oil composition is shown.[1]

$$\overline{x_i} = \frac{\sum_{B_{sp,o}} z_i + \sum_{B_{tp}} x_i}{n_{sp,o} + n_{tp}} \tag{5.17}$$

Here $\overline{x_i}$ is the upscaled mole fraction of component i in the oil phase, $B_{sp,o}$ are the single-phase oil blocks and B_{tp} are the two-phase blocks. $n_{sp,o}$ and n_{tp} are the number of single-phase oil and two-phase blocks respectively.
The upscaling method for the gas phase is analogous as shown in (5.18).

$$\overline{y_i} = \frac{\sum_{B_{sp,g}} z_i + \sum_{B_{tp}} y_i}{n_{sp,g} + n_{tp}} \tag{5.18}$$

From the upscaled mole fraction, the source term in the vapor-liquid equilibrium equation can be determined using (5.19).

$$\Delta f_i = \overline{y_i} - K_i \cdot \overline{x_i} \tag{5.19}$$

For each coarse grid block the source terms are tabulated versus z_1. If the coarse block is in single-phase the source terms are set to zero otherwise equation (5.19) is used. The source terms for the initial composition and injection composition are added to the table as well.

5.4 Coarse simulation using source term table

In the coarse simulation, the source term to be used in the negative flash is determined for each grid block in each time step. This is done using the tables of source terms versus z_1 and the composition in the grid block from the previous time step. The source term tables for each grid block can be used directly for the coarse simulation. This is considered as global upscaling.

With the tables of the source term a correlation can be made for the source term df versus the composition. This correlation can then be used in the coarse simulation. This can be seen as the local-global upscaling step. In this research this correlation is obtained from the whole reservoir and applied to the whole reservoir. To save on simulation time for other cases it is possible to run a smaller fine scale simulation in order to obtain this correlation and apply it to the whole reservoir.

5.5 Optimizing source term correlation

To quantify the error between the upscaled fine scale result and the coarse scale simulation the misfit value f is used. The misfit value is defined as (5.20) with $S_{g,C}$ the coarse scale saturation distribution and $S_{g,f}$ the upscaled fine scale saturation distribution.

$$f = \sum_i \left(S_{g,C}(i,t) - S_{g,f}(i,t) \right)^2 \tag{5.20}$$

The misfit value can also be used to optimize the correlation for the source term. For the optimization procedure the correlation for the source term needs to be parameterized. Changing the parameters results in a different correlation for the source term and thereby a different saturation distribution. The correlation for the source term that gives a minimal value for the misfit between the saturation distributions will be considered the best correlation.

To minimize the misfit value by changing the parameters of the correlation, the fmincon function in Matlab is used. The parameters can be constrained to prevent non-physical compositions in the simulation. The fmincon functions from Matlab attempts to find a constrained minimum of a scalar function of several variables starting at an initial estimate. This is generally referred to as constrained nonlinear optimization or nonlinear programming [45]. For this optimization the scalar function is (5.20) and the variables are the parameters that describe the correlation between the source term and composition. The algorithm used in the fmincon function is the ‘interior-point’ algorithm. This algorithm is described in details by Byrd, Gilbert [46], Byrd, Hribar [47] and Waltz, Morales [48].

6 Results

In this chapter the results of the different simulations are shown. The main results are presented by a comparison between the gas saturation distribution of the fine-scale and coarse scale simulation. The fine scale distribution is the averaged fine scale value over the coarse block. This averaged fine scale value is used to compare with the coarse scale distribution. Finally an optimization is performed to improve the results of the simulation using a correlation of the parameterized source terms.

6.1 Simulation without thermodynamics

First, the fine scale and coarse scale simulations are run for an effectively binary system to check the upscaling of the permeabilities and relative permeabilities. The binary system is achieved by making the medium component close to zero in both the injection gas and the initial fluid. This results effectively in a binary system but is not a true binary system. A true binary system would consist out of just two components. Because the medium component is "left out" there are little thermodynamic effects. The heavy and light component stay in the oil and gas phase respectively at the used pressure and temperatures.

The compositions and K-values used for the injection gas and the initial fluid are shown in Table 1. The injection gas composition and the initial oil composition are set at the dew and bubble point respectively. By setting the value for the second component the whole composition can be calculated using the K-values and dew point or bubble point equations given by (6.1) and (6.2) respectively.

$$\sum_i \frac{y_i}{K_i} = 1 \tag{6.1}$$

$$\sum_i x_i K_i = 1 \tag{6.2}$$

The three components are methane, C_1, normal butane, NC_4, and decane, C_{10}.

Table 1 Compositions and K-values used in the binary simulation

Component	Injection	Initial	K-values
C_1	0.9595	0.3818	2.5
NC_4	0.01	0.01	1.5
C_{10}	0.0305	0.6082	0.05

Because of an error discovered afterwards, the initial composition does not correspond with a bubble point composition. At the time of this discovery there was no time to correct this error and use a different composition. This error and the use of this composition does not influence the validity of the results. The initial composition is in the single-phase oil regime because $\sum_i x_i K_i < 1$. The composition was set at bubble point only as a way to choose a composition.

The saturation distribution that resulted from the simulation is shown with the red line in Figure 9 together with the upscaled fine scale saturation distribution represented by the blue line. The y-axis represents the gas saturation and the x-axis is the grid block number.

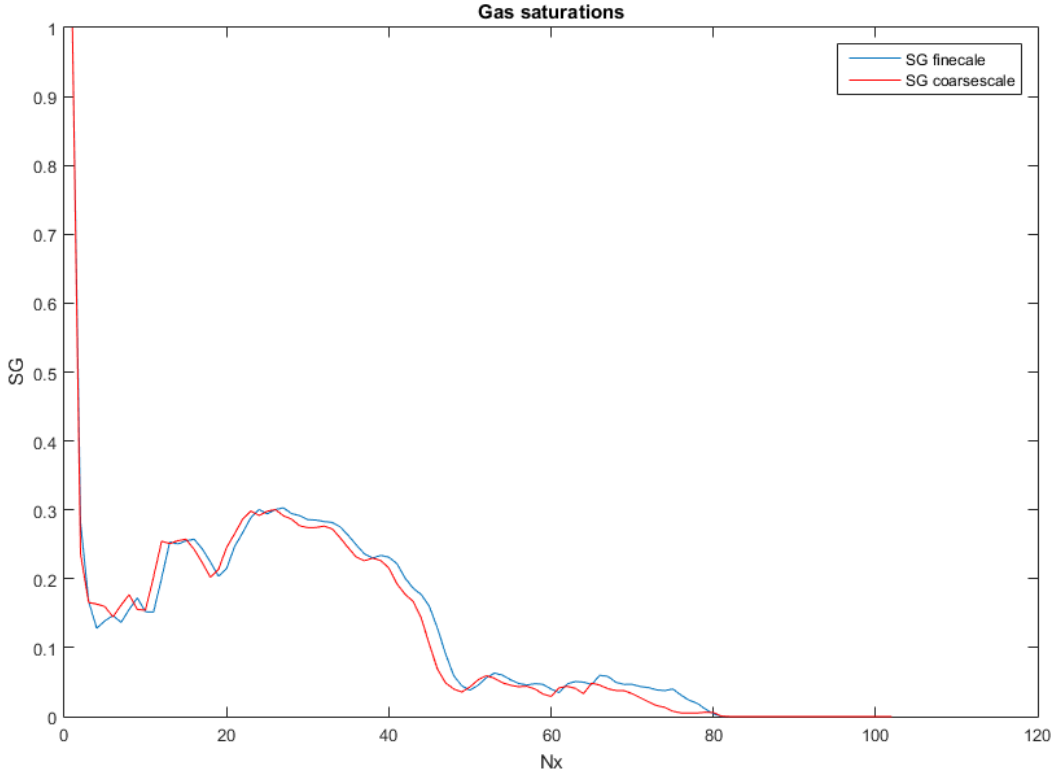

Figure 9 Gas saturation distribution for binary system. No thermodynamic correction was performed.

The gas saturation distributions shown in Figure 9 show how the gas is distributed over the reservoir. At the left side in grid block 1, the gas is injected and the oil is produced at grid block 102 on the right side. The graph shows there is no gas breakthrough yet.

The misfit value calculated using (5.20) is given in (6.3). The saturation distributions in Figure 9 look very similar and the misfit value is reasonable. Based on this, it is concluded that the simulation without any thermodynamics being involved works correctly.

$$f_{binary} = 0.3087 \tag{6.3}$$

6.2 Non-Equilibrium thermodynamic correction

Now the upscaling of the permeabilities and relative permeabilities is shown to be working for a binary system, the next step is to introduce the thermodynamic effects and apply an upscaling procedure that takes those thermodynamic effects into account. A new composition for the injection gas and initial fluid is chosen to introduce the thermodynamic effects. The compositions are shown in Table 2 together with the K-values. The composition for the injection gas is chosen to be almost purely methane. The initial oil composition is set at its bubble point. The value for the second component, CO_2, is set at 0.3. Given that the composition is at bubble point and known K-values the full composition can be calculated using (6.2). The three components are methane, C_1, carbon dioxide, CO_2, and decane, C_{10}.

Table 2 Injection and initial compositions for simulation with thermodynamic effects

Component	Injection	Initial	K-values
C_1	0.98	0.08707	2.5
CO_2	0.01	0.3000	1.5
C_{10}	0.01	0.6122	0.05

The same error in the calculation of the initial composition for the binary simulation caused the initial composition in Table 2 not to be a bubble point composition. Again, this does not influence the validity of the presented results. The initial composition is in the single-phase oil regime because $\sum_i x_i K_i < 1$.

With the thermodynamic effects present, a correction to the phase equilibrium assumptions is needed. This correction needs to account for the tilting of the tie-lines as the composition changes. The slope of the tie-lines represents the K-value in the thermodynamic equilibrium equation. An example of these tilting tie-lines is shown in Figure 10.

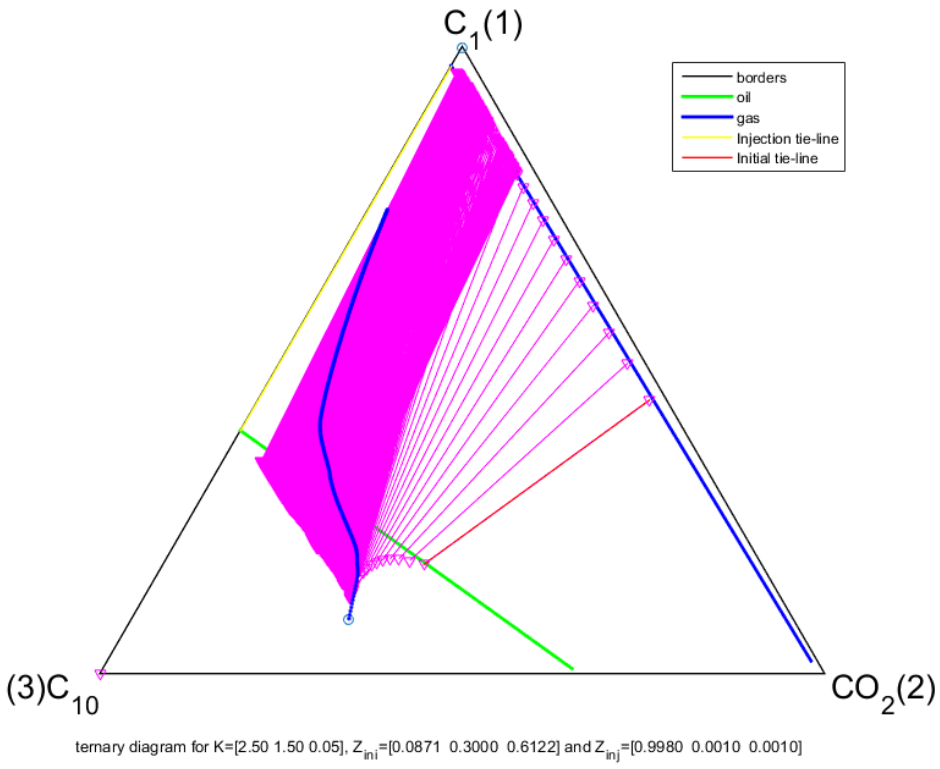

Figure 10 Ternary plot showing the tilting tie-lines in pink. The blue dots represent the coarse scale compositions.

In Figure 10 all the tie lines from the simulation are shown. The tie-lines quickly tilt away from the initial tie-line and tilt slowly towards the injection tie-line. The coarse scale compositional path, represented by the blue dots in Figure 10, follows the new set of tilted tie-lines. In Figure 11 fewer tie-lines are plotted together with the coarse scale compositions. This shows the coarse composition following the tilted tie-lines much clearer.

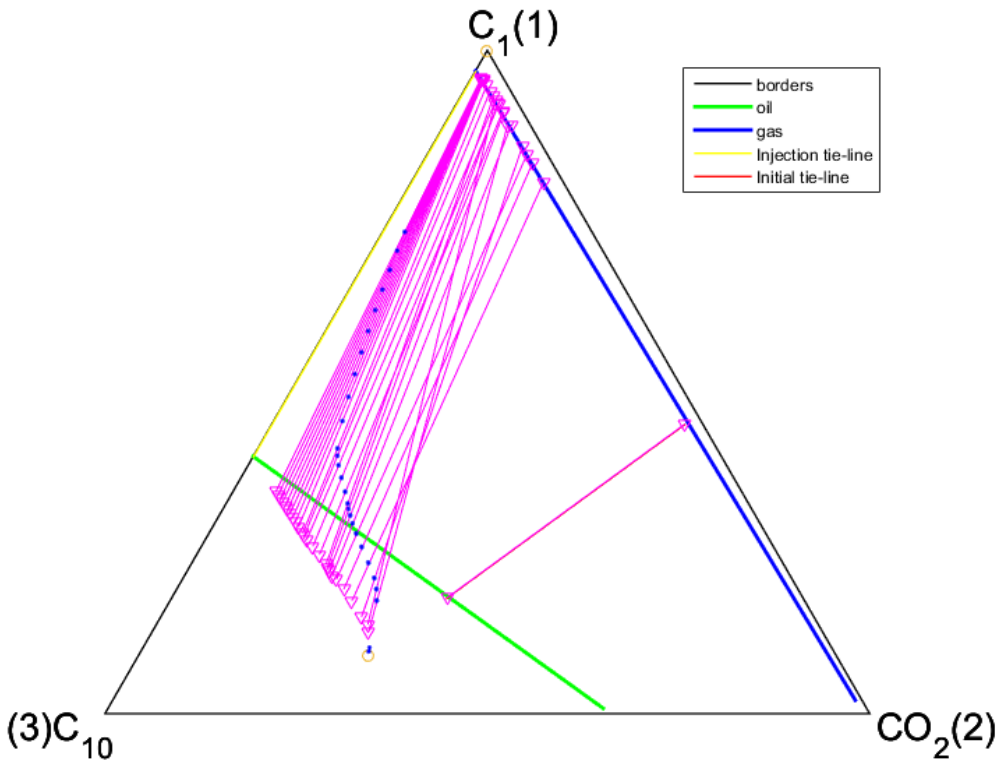

ternary diagram for K=[2.50 1.50 0.05], Z_{ini}=[0.0871 0.3000 0.6122] and Z_{ini}=[0.9980 0.0010 0.0010]

Figure 11 Ternary plot showing some of the tilting tie-lines in pink together with the coarse scale compositions represented by the blue dots.

In Figure 12 all the source terms of the three components for all grid blocks at all time steps, to compensate for the tilting tie-lines, are plotted. These source terms are used to run a coarse simulation, the gas saturation distribution of this simulation is shown in Figure 13 with the red line.

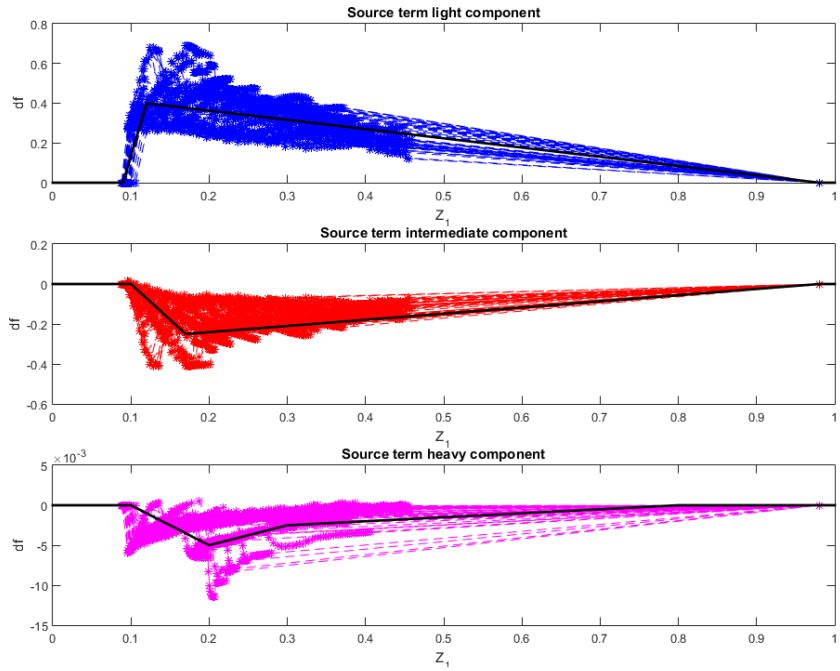

Figure 12 Source term df versus Z1 for the three components with the black line the correlation used in coarse simulation

The black line is a correlation made for all the grid blocks and is used for another coarse scale simulation. The values of the correlations are shown in (6.4). The results of this simulation are shown with the black line in Figure 13.

$$\begin{aligned} Z_1 &= [0,\ 0.09,\ 0.12,\ 0.98,\ 1] \\ df_1 &= [0,\ 0,\ 0.4,\ 0,\ 0] \\ Z_2 &= [0,\ 0.1,\ 0.17,\ 0.98,\ 1] \\ df_2 &= [0,\ 0,\ -0.25,\ 0,\ 0] \\ Z_3 &= [0,\ 0.1,\ 0.2,\ 0.3,\ 0.8,\ 1] \\ df_3 &= [0,\ 0,\ \text{-}0.005,\ \text{-}0.0025,\ 0,\ 0] \end{aligned} \tag{6.4}$$

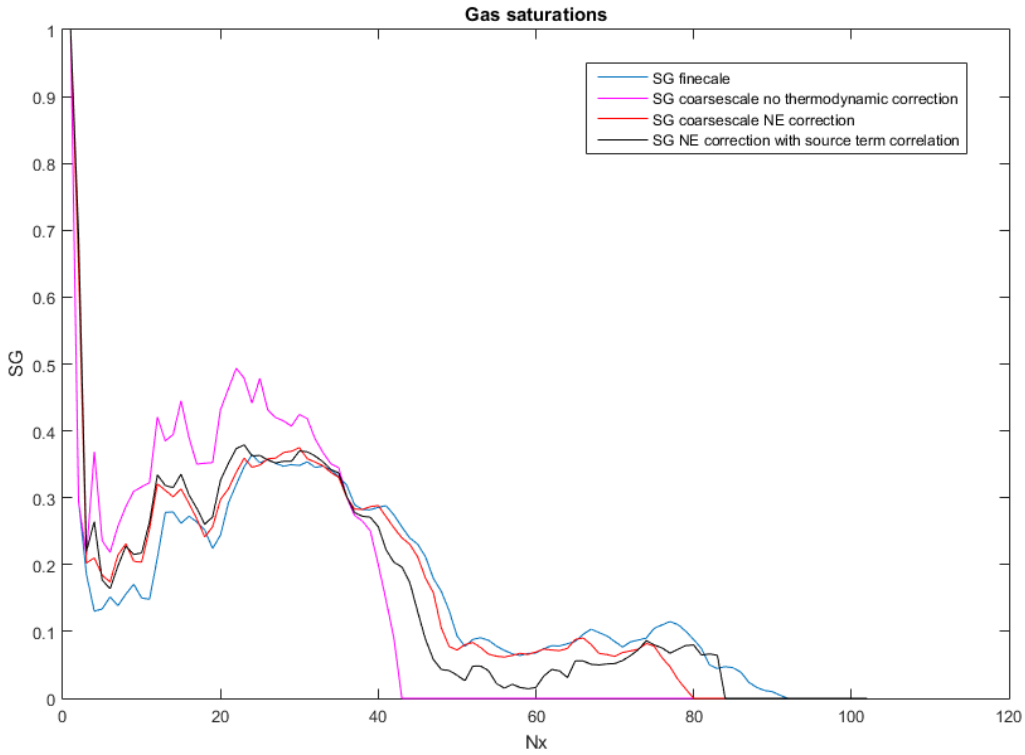

Figure 13 Saturation distribution with the blue line the average fine-scale distribution, the pink line represents the saturation distribution for a coarse simulation without a thermodynamic correction, the red line the coarse scale distribution with the original sourceterms for each grid block and the black line the course scale distribution obtained using the correlation shown in Figure 12.

The gas saturation distribution without the Non-Equilibrium(NE) correction is shown by the pink line in Figure 13. Without the NE correction the gas does not go through the reservoir as far as the upscaled fine scale result. The gas bulks up in roughly the first 40 grid blocks. With the NE correction the gas reaches further into the reservoir and results in a similar gas distribution as the upscaled fine scale result.

To quantify these results the misfit value is used as given by equation (5.20). The value for no thermodynamic correction is given by (6.5) while the value for the NE correction using the source term tables is (6.6). When using the shown correlation in Figure 12 this values increases to (6.7).

$$f_{\text{No correction}} = 1.1121 \tag{6.5}$$

$$f_{\text{NE correction}} = 0.2445 \tag{6.6}$$

$$f_{\text{Fit}} = 0.3731 \tag{6.7}$$

To improve the results, an optimization procedure is performed, the results of this optimization will be shown in section 6.3.

When using the second permeability field as defined in chapter 4, a different saturation distribution is obtained. This can be seen in Figure 14. The source terms for the second permeability field are plotted versus the component Z_1 to make a correlation. This is shown in Figure 15.

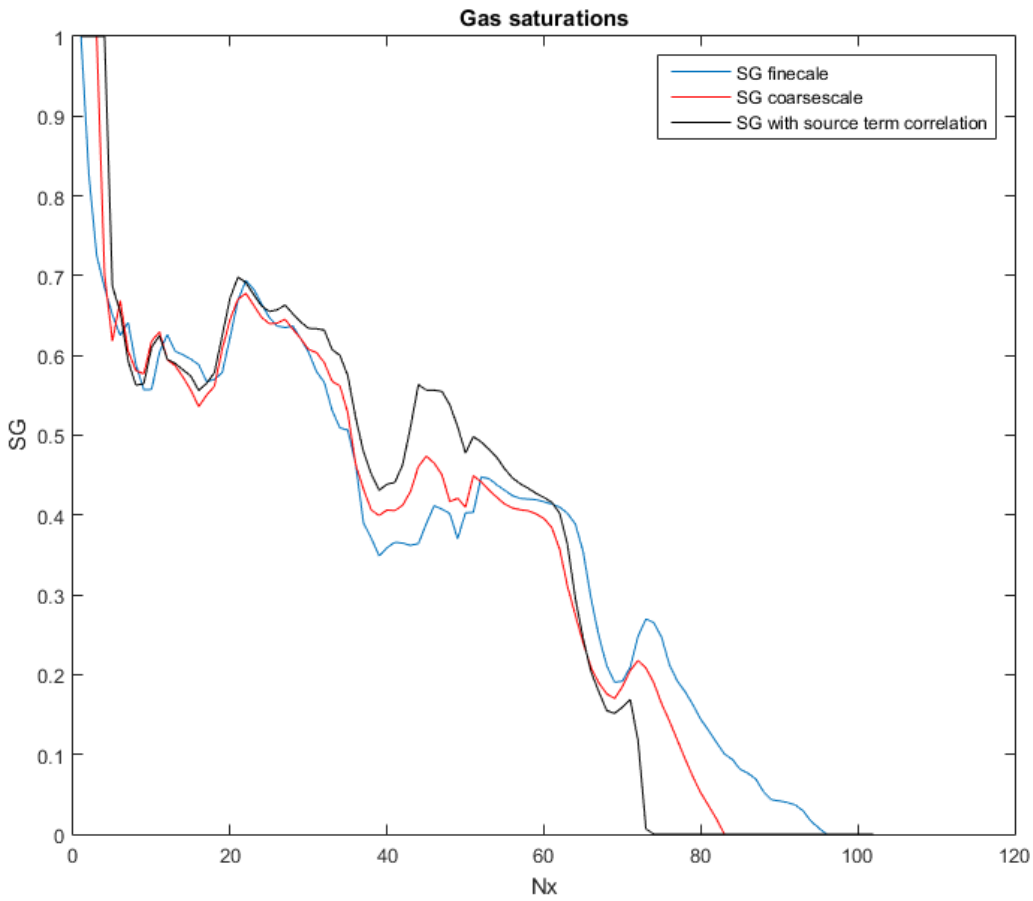

Figure 14 Saturation distribution for the second permeability distribution with the blue line representing the averaged finescale saturation distribution, the red line the coarse scale distribution using the tables and the black line the coarse simulation distribution using the correlation

The red line in Figure 14 represents the coarse simulation with the source terms of every grid block and the black line represents the coarse simulation using the correlation of the source term as shown in Figure 15. The misfit value given in (6.8), for the red curve that used the full source term table is a bit higher than for the first permeability distribution.

$$f = 0.3419 \tag{6.8}$$

The misfit value given in (6.9), for the correlation shown in Figure 15 is a lot bigger and shows this correlation can be improved a lot. However, in this research this will not be investigated, only an optimization procedure for the first reservoir will be explored.

$$f = 0.9868 \tag{6.9}$$

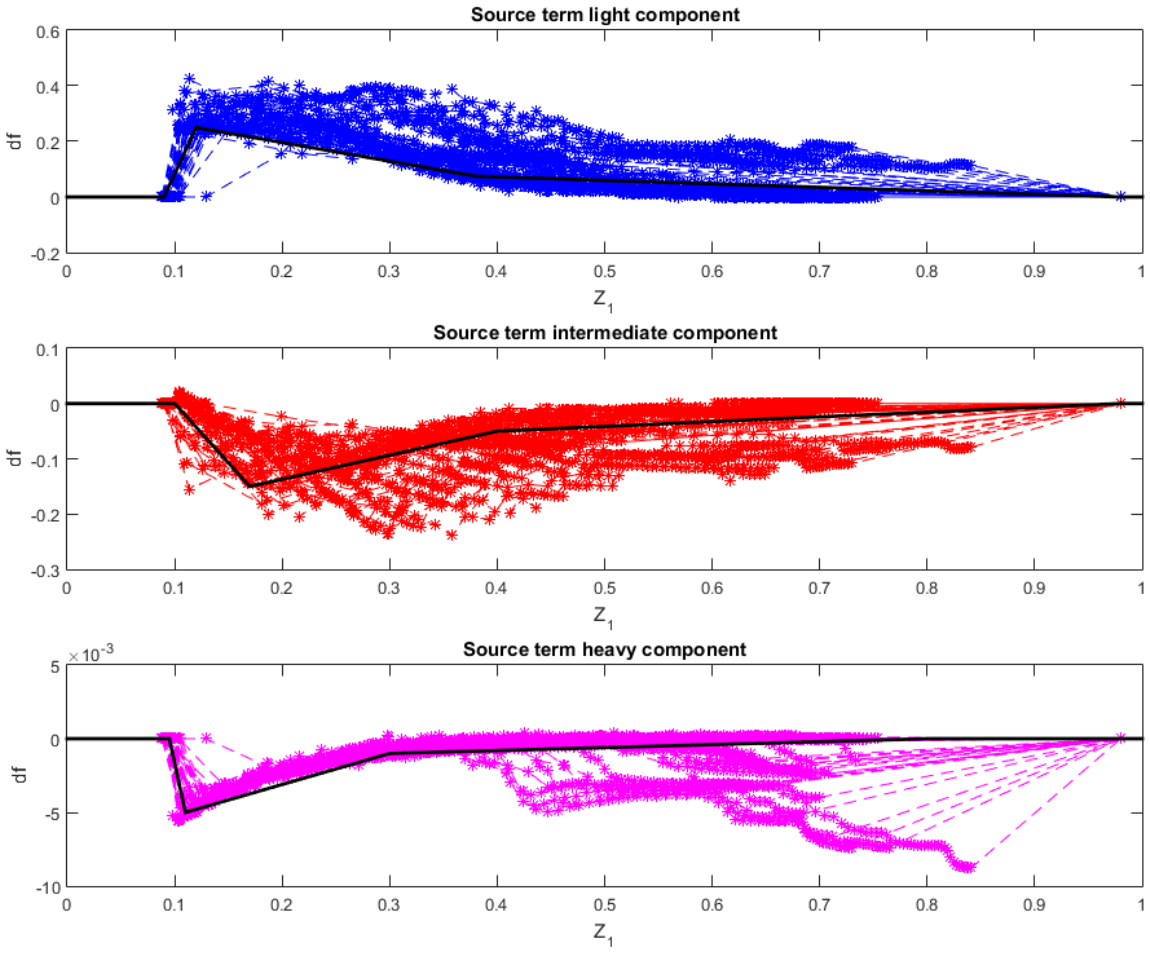

Figure 15 Source terms versus Z1 for the three components

6.3 Optimization of source term correlation

The optimization was performed for the first permeability distribution. For this optimization the correlations are parameterized. The correlation consists points connected with linear lines. The parameters of the correlation are the coordinates of points along the correlation.

6.3.1 Optimization 1

For the first optimization only three parameters are used, one for each correlation. The values for the initial guess are given below by (6.10).

$$
\begin{aligned}
Z_1 &= [0,\ 0.09,\ 0.12,\ 0.98,\ 1] \\
df_1 &= [0,\ 0,\ \text{Fit0}(1),\ 0,\ 0] \\
Z_2 &= [0,\ 0.1,\ 0.17,\ 0.98,\ 1] \\
df_2 &= [0,\ 0,\ \text{Fit0}(2),\ 0,\ 0] \\
Z_3 &= [0,\ 0.1,\ 0.2,\ 0.8,\ 1] \\
df_3 &= [0,\ 0,\ \text{Fit0}(3),\ 0,\ 0]
\end{aligned}
\tag{6.10}
$$

With the Fit0 vector given as (6.11).

$$\text{Fit0} = [0.400,\ -0.250,\ -0.005] \tag{6.11}$$

The misfit value for gas saturation distributions for this initial guess is given in (6.12).

$$f = 0.3855 \tag{6.12}$$

Optimizing this initial guess gives a Fit vector given by (6.13).

$$\text{Fit} = [0.4724,\ -0.3411,\ -0.0198] \tag{6.13}$$

For this optimization the parameters are constrained by the upper constraint U_c given in (6.14) and the lower constraint L_c given in (6.15).

$$U_c = [1,\ 0,\ 0] \tag{6.14}$$

$$L_c = [0,\ -0.5,\ -0.1] \tag{6.15}$$

The misfit value for gas saturation distribution of this optimized result is given by (6.16).

$$f = 0.2487 \tag{6.16}$$

The initial guess (green line) and the optimized correlation (black line) are shown in Figure 16 below. The saturation distribution obtained from the coarse scale simulation using the optimized correlation is compared in Figure 17.

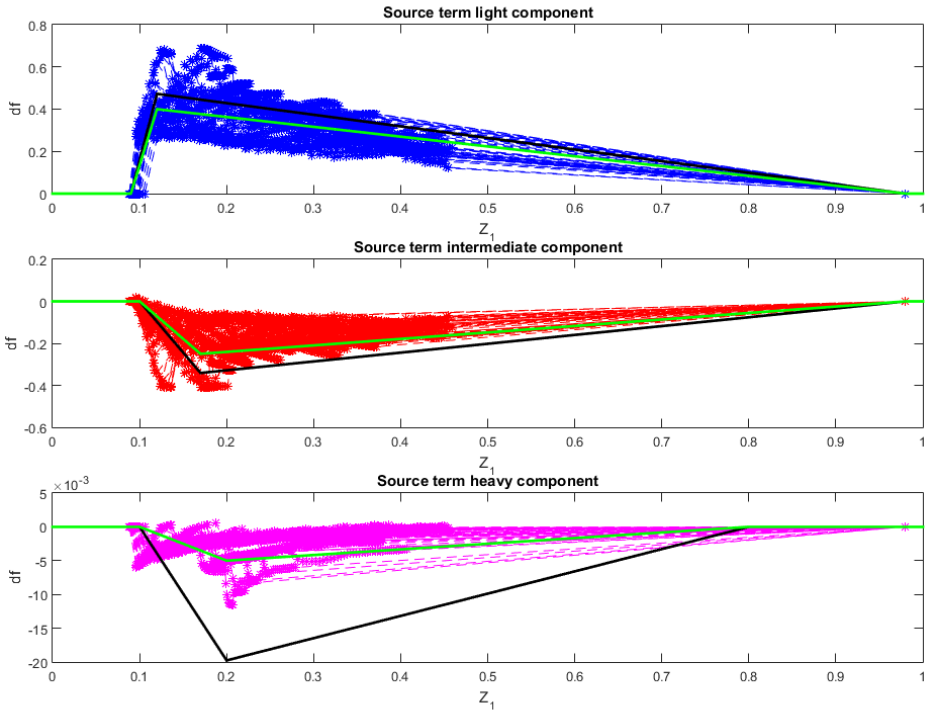

Figure 16 source term graphs with the green line the initial guess and the black line the optimized correlation

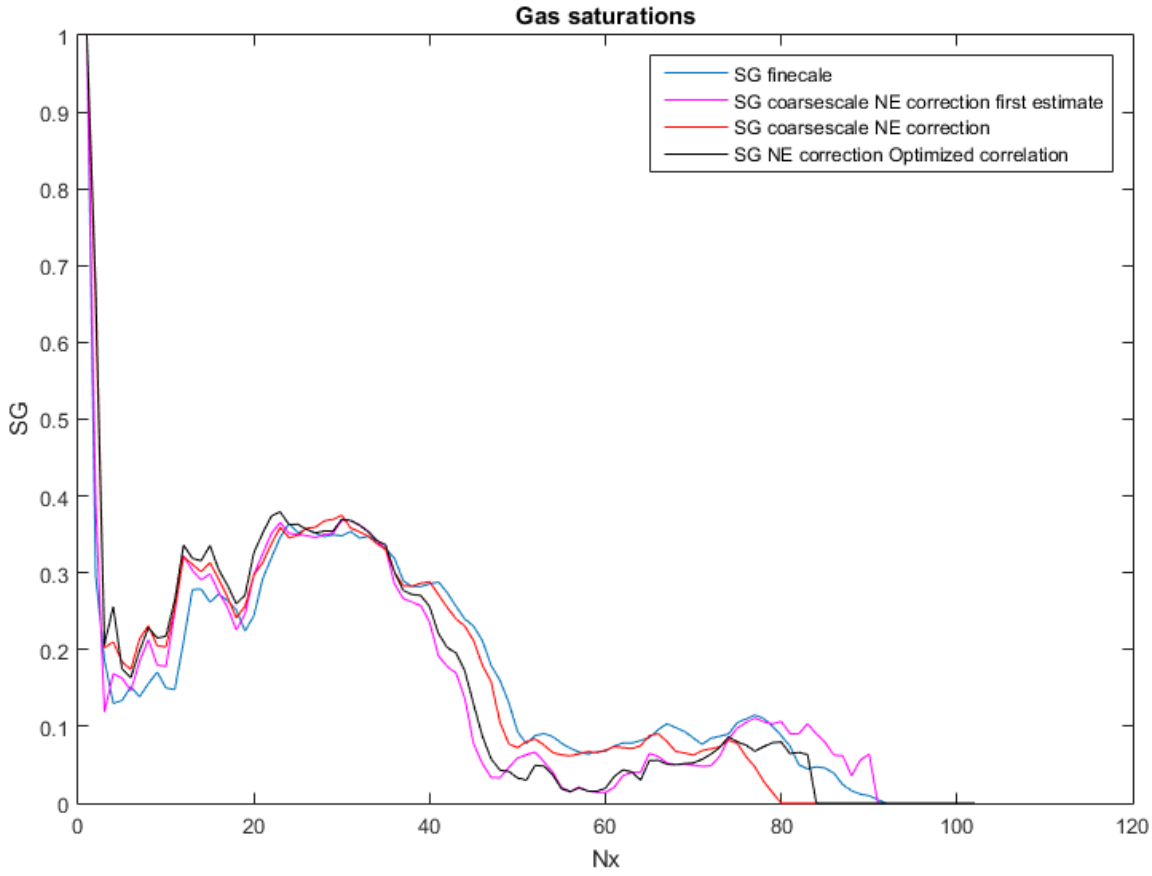

Figure 17 Gas saturation distributions comparison between upscaled finescale, NE-correction using full table, NE-correction initial guess correlation and NE-correction using the optimized correlation.

6.3.2 Optimization 2

The optimized parameter for the third component seems to be an outlier compared to the values obtained from the fine scale simulation. A new optimization with an extra parameter in the correlation is done to see if this improves the result and does not result in outliers in the optimized correlation.

The initial guess for the first and second component are based on the optimized result from before. For the third component another parameter is added. The full initial guess is shown below in (6.17).

$$\begin{aligned} Z_1 &= [0,\ 0.09,\ 0.12,\ 0.98,\ 1] \\ df_1 &= [0,\ 0,\ \mathrm{Fit0}(1),\ 0,\ 0] \\ Z_2 &= [0,\ 0.1,\ 0.17,\ 0.98,\ 1] \\ df_2 &= [0,\ 0,\ \mathrm{Fit0}(2),\ 0,\ 0] \\ Z_3 &= [0,\ 0.1,\ 0.12,\ 0.2,\ 0.8,\ 1] \\ df_3 &= [0,\ 0,\ \mathrm{Fit0}(3),\ \mathrm{Fit0}(4)\ 0,\ 0] \end{aligned} \tag{6.17}$$

With the $\mathrm{Fit0}$ vector given as (6.18).

$$\mathrm{Fit0} = [0.4724,\ -0.3411,\ -0.005,\ -0.005] \tag{6.18}$$

The misfit value for this initial guess is:

$$f = 0.3482 \tag{6.19}$$

The resulting saturation distribution of this initial guess is very similar to the distribution from the previously optimized result as can be seen in Figure 18.

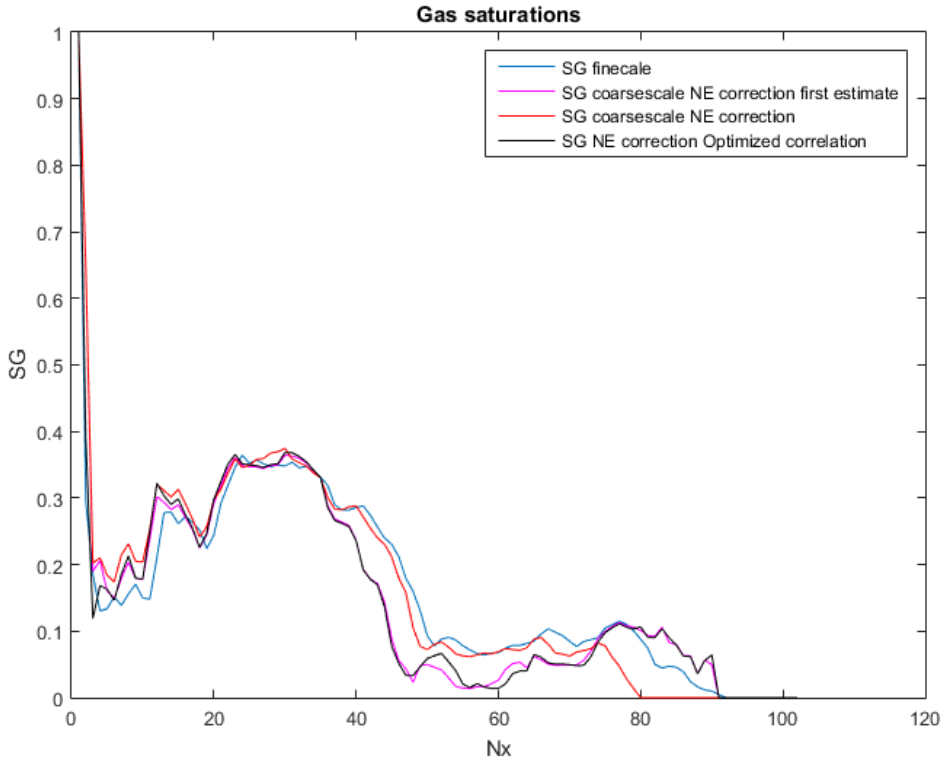

Figure 18 Saturation distribution comparison between the new initial guess and first optimized correlation.

Optimizing this initial guess gives a Fit vector given by (6.20). For this optimization the parameters are constrained by the upper constraint U_c given in (6.21) and the lower constraint L_c given in (6.22).

$$\text{Fit}=\left[0.5384,\ -0.3447,\ -0.0506,\ -0.0704\right] \tag{6.20}$$

$$U_c=\left[1,\ 0,\ 0,\ 0\right] \tag{6.21}$$

$$L_c=\left[0,\ -0.5,\ -0.1,\ -0.1\right] \tag{6.22}$$

The misfit value for this optimized result is shown in (6.23).

$$f=0.3443 \tag{6.23}$$

The resulting correlation from this optimization is shown in Figure 19 and the saturation distribution is compared in Figure 20.

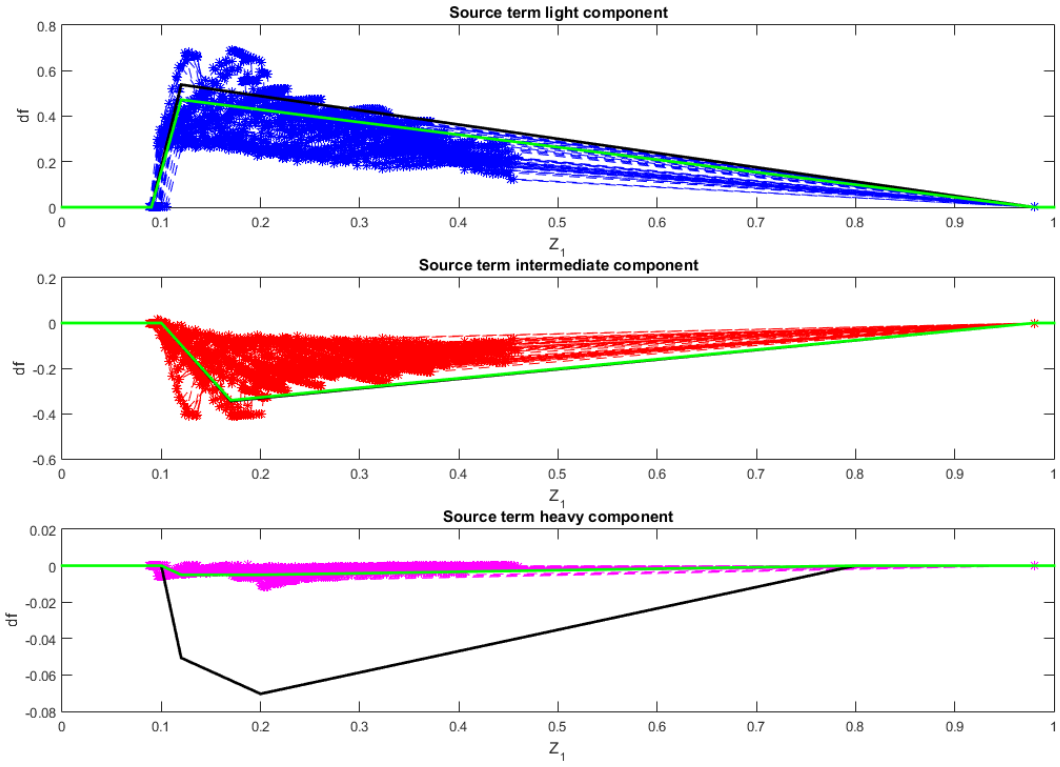

Figure 19 Source term graphs with initial guess correlation and optimized correlation for optimization 2.

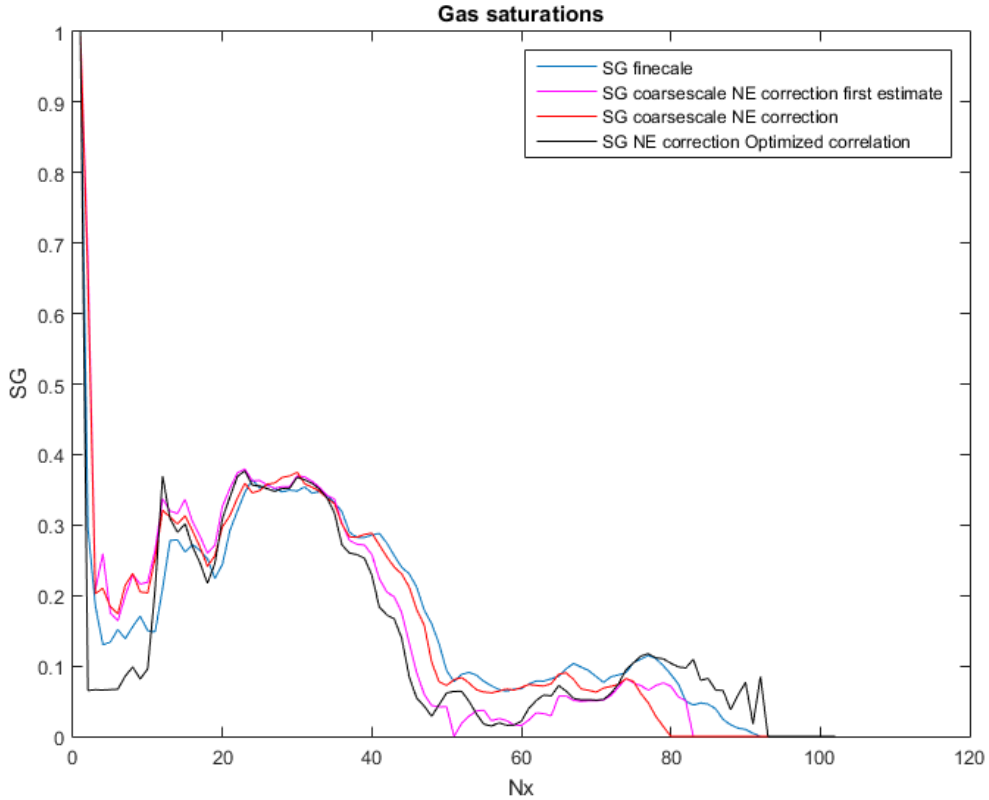

Figure 20 Saturation distribution comparison between the initial guess and correlation from optimization 2.

6.3.3 Optimization 3

Again, an attempt is made to improve the correlation for the third component. Now one point is allowed to move in a 2D plane so the Z_1-value and the df value are allowed to change. This leads to again a total of 4 parameters. The initial guess is shown in (6.24)

$$\begin{aligned} Z_1 &= [0,\ 0.09,\ 0.12,\ 0.98,\ 1] \\ df_1 &= [0,\ 0,\ \mathrm{Fit0}(1),\ 0,\ 0] \\ Z_2 &= [0,\ 0.1,\ 0.17,\ 0.98,\ 1] \\ df_2 &= [0,\ 0,\ \mathrm{Fit0}(2),\ 0,\ 0] \\ Z_3 &= [0,\ 0.1,\ \mathrm{Fit0}(3),\ 0.8,\ 1] \\ df_3 &= [0,\ 0,\ \mathrm{Fit0}(4)\ 0,\ 0] \end{aligned} \tag{6.24}$$

With the $\mathrm{Fit0}$ vector given as:

$$\mathrm{Fit0}=[0.4724,\ -0.3411,\ 0.15,\ -0.005] \tag{6.25}$$

The values for $\mathrm{Fit0}(1)$ en $\mathrm{Fit0}(2)$ are based on the result of the first optimization since it gave the best result. The misfit value for this initial guess is given as (6.26).

$$f = 0.3519 \tag{6.26}$$

The optimization resulted in the values in (6.27). For this optimization the parameters are constrained by the upper constraint U_c given in (6.28) and the lower constraint L_c given in (6.29).

$$\mathrm{Fit}=[0.5253,\ -0.3285,\ 0.1460,\ -0.0210] \tag{6.27}$$

$$U_c = [1,\ 0,\ 0.79,\ 0] \tag{6.28}$$

$$L_c = [0,\ -0.5,\ 0.11,\ -0.1] \tag{6.29}$$

$$f = 0.3252 \tag{6.30}$$

The first guess and optimized correlations are shown in Figure 21 and the corresponding saturation distributions are shown in Figure 22.

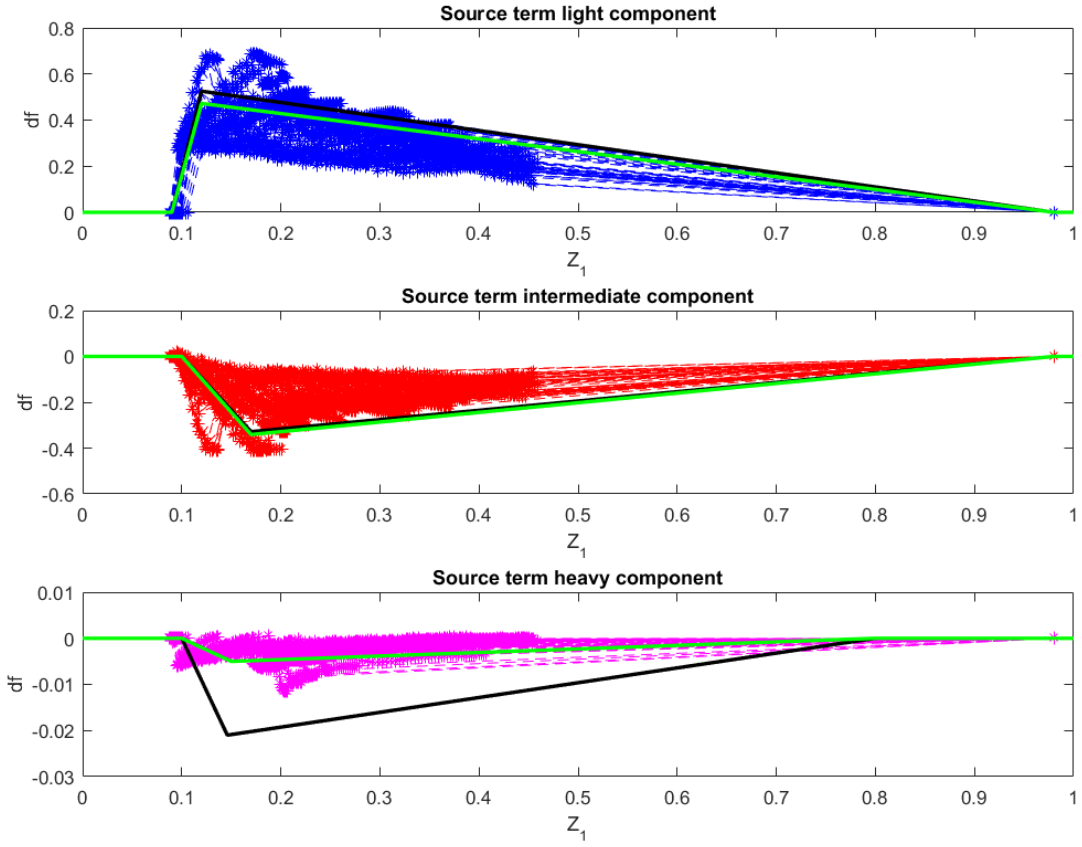

Figure 21 Source term graphs with initial guess correlation and optimized correlation for optimization 3.

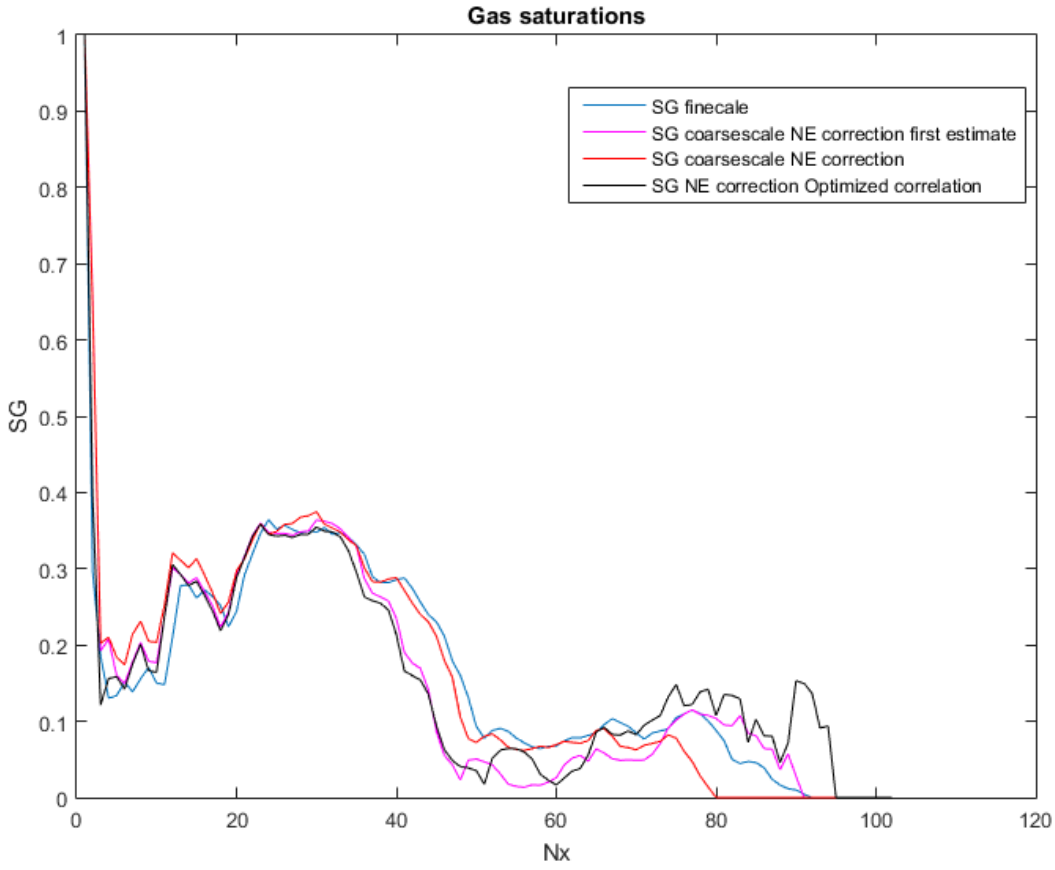

Figure 22 Saturation distribution comparison between the initial guess and correlation from optimization 3.

6.3.4 Optimization 4

This optimization was performed to see if the optimization for a different time step would give a very different result. Instead of comparing the saturations at t=100% the saturation are now compared at t=60%. For t=100% is considered the 500 day duration of the simulation, t=60% would be after 300 days. For this optimization the values from the first optimization are used again.

The same parameterization as shown in (6.10) is used, but $\mathrm{Fit0}$ is now used with the values from (6.13) as shown in (6.31).

$$\mathrm{Fit0}=\left[0.4724,\ -0.3411,\ -0.0198\right] \tag{6.31}$$

At t=60% this gives a misfit value of:

$$f = 0.3215 \tag{6.32}$$

The values of Fit0 are optimized to the values shown in (6.33). The upper and lower constraints are given by (6.14) and (6.15) respectively.

$$\mathrm{Fit}=\left[0.3957,\ -0.1408,\ -0.0296\right] \tag{6.33}$$

The misfit value f=0.1335 at t=60% and at t=100% the misfit value is f=0.2314. Both are an improvement on the first optimization.

$$f = 0.2314, \text{ at } t = 100\%$$
$$f = 0.1335, \text{ at } t = 60\% \tag{6.34}$$

The optimized correlation and first guess are shown in Figure 23. The saturation distributions at t=60% are shown in Figure 24 and for t=100% in Figure 25.

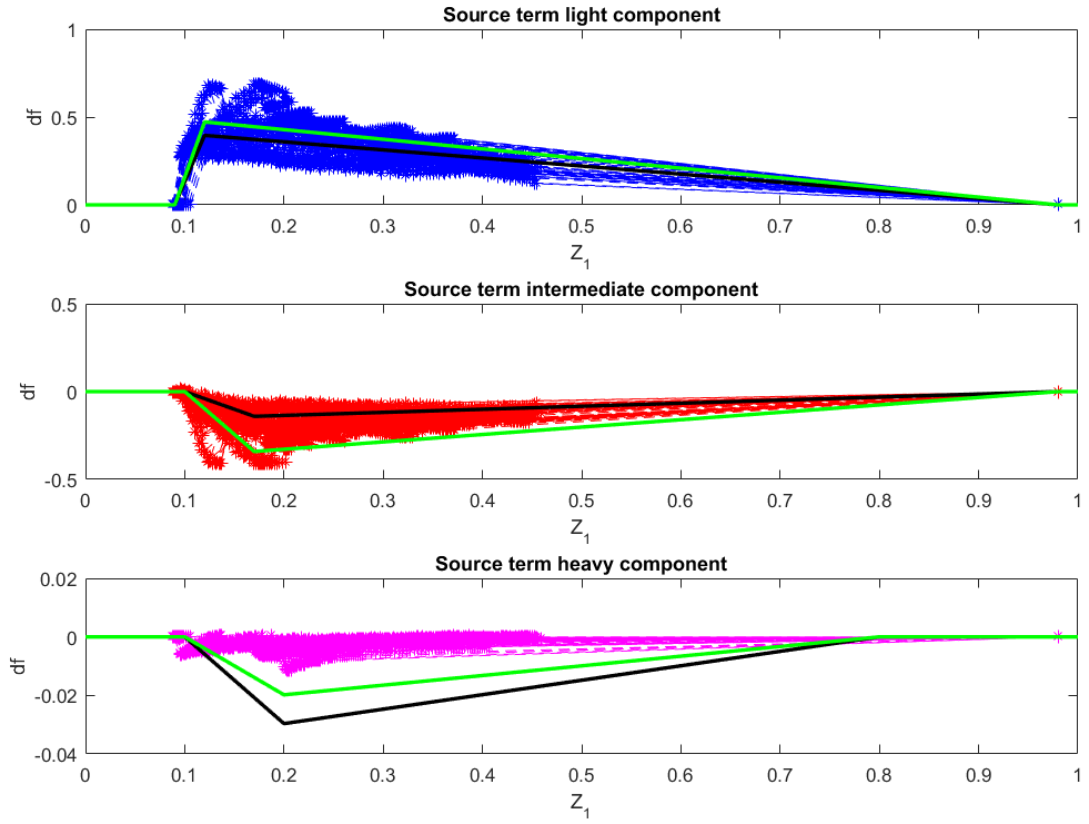

Figure 23 Source term graphs with initial guess correlation and optimized correlation for optimization 4.

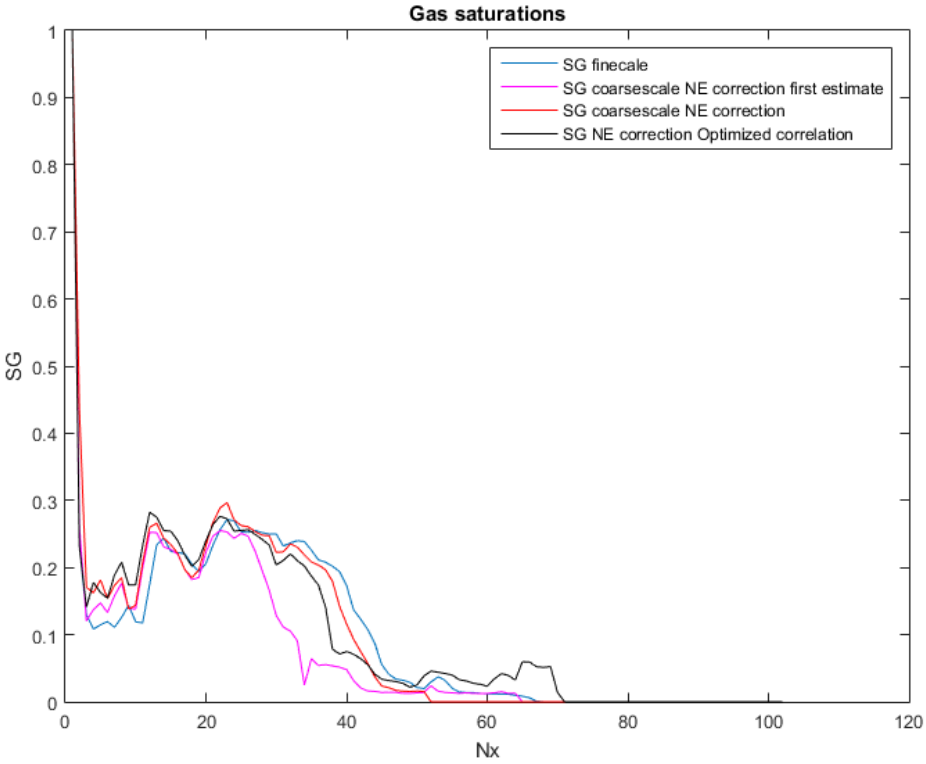

Figure 24 Comparison of gas saturation distributions at t=60% for upscaled finescale, NE-correction using source term tables. NE-correction using initial guess correlation for sourceterm and the NE-correction using the optimized correlation for the sourceterm.

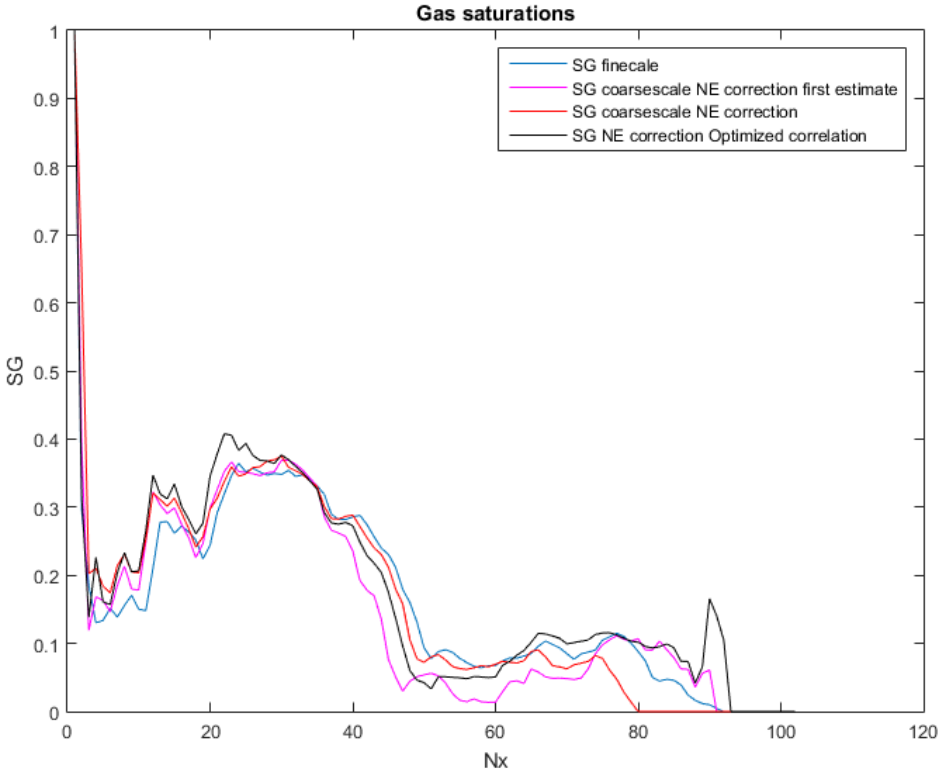

Figure 25 Saturation distribution comparison between the initial guess and correlation from optimization 4.

6.3.5 Optimization 5

Because each new optimization was done on top of the results of the first optimization a check is needed if this is of influence on the results. Now the optimization is performed like the first optimization but with the results of the first optimization as input.

The values from (6.10) and (6.31) are used and the parameters are constrained by (6.14) and (6.15). This results in the optimized values that are given by (6.35).

$$\text{Fit}=\left[0.3916,\ -0.1692,\ -0.0299\right] \tag{6.35}$$

And the misfit value f = 0.2013 and for comparison with the optimization results at t=60% the misfit value f=0.1767.

$$\begin{aligned} f &= 0.2013,\ \text{at } t = 100\% \\ f &= 0.1767,\ \text{at } t = 60\% \end{aligned} \tag{6.36}$$

These give a better result based on the misfit value f. Also, these values are pretty similar to the ones found for the optimization at t=60%.

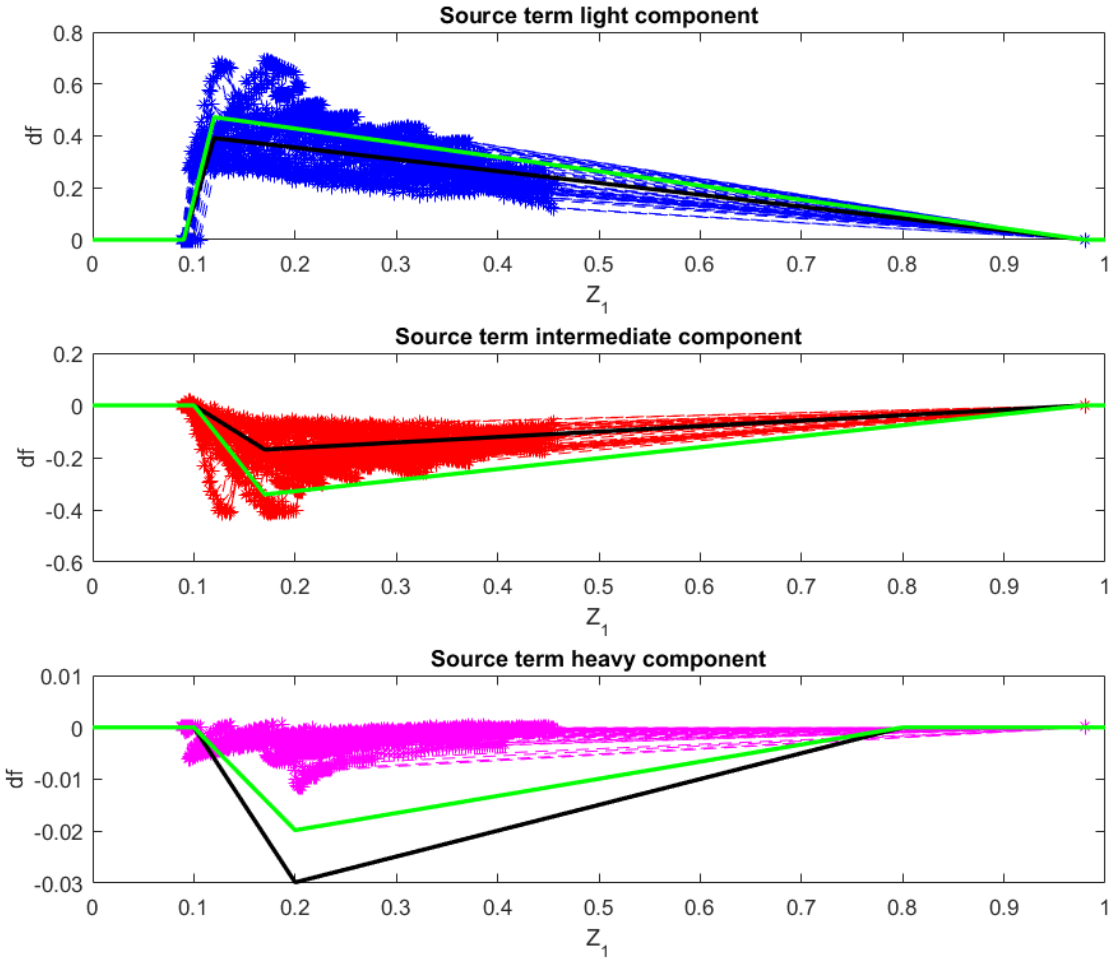

Figure 26 Source term graphs with initial guess correlation and optimized correlation for optimization 5.

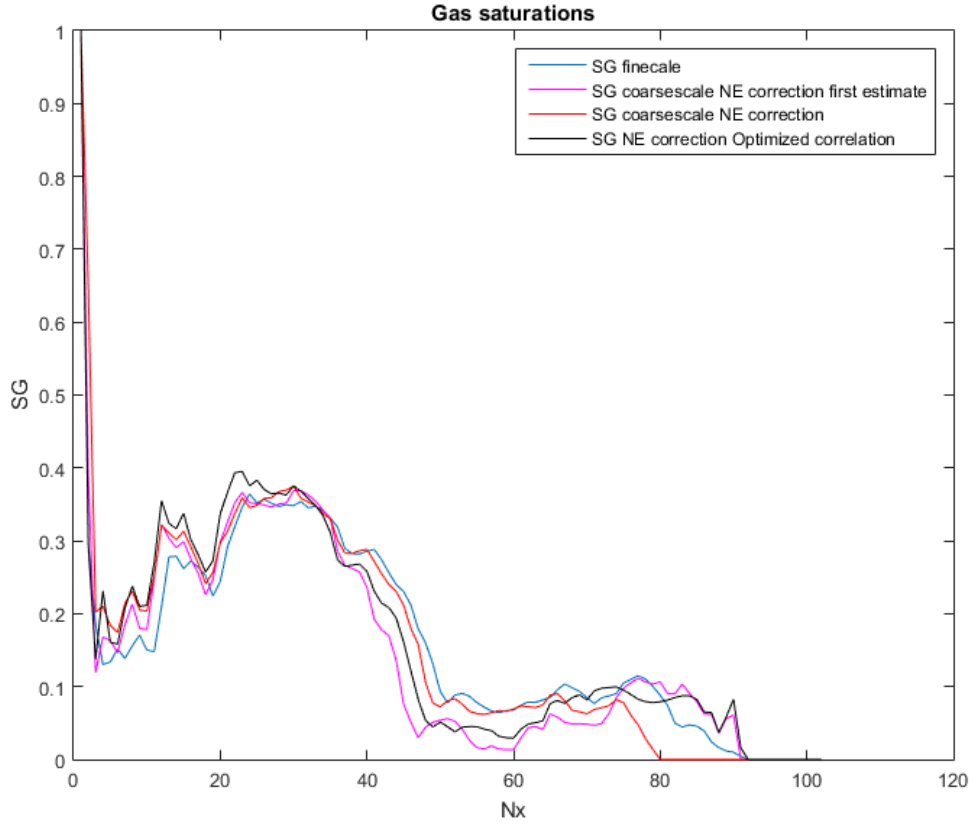

Figure 27 Saturation distribution comparison between the initial guess and correlation from optimization 5.

6.3.6 Optimization 6

One more attempt is made to improve the correlation for the third component using the values from previous optimization for the first and second component and now have three parameters for the correlation of the third component. The one point is only allowed to change in y-axis and the second in a 2D-plane. The values for the initial guess are shown in (6.37) and (6.38).

$$\begin{aligned} Z_1 &= [0,\ 0.09,\ 0.12,\ 0.98,\ 1] \\ df_1 &= [0,\ 0,\ \mathrm{Fit0}(1),\ 0,\ 0] \\ Z_2 &= [0,\ 0.1,\ 0.17,\ 0.98,\ 1] \\ df_2 &= [0,\ 0,\ \mathrm{Fit0}(2),\ 0,\ 0] \\ Z_3 &= [0,\ 0.1,\ 0.11\ \mathrm{Fit0}(4),\ 0.8,\ 1] \\ df_3 &= [0,\ 0,\ \mathrm{Fit0}(3)\ \mathrm{Fit0}(5)\ 0,\ 0] \end{aligned} \tag{6.37}$$

$$\mathrm{Fit0} = [0.3916,\ -0.1692,\ -0.005\ 0.200\ -0.005] \tag{6.38}$$

The misfit value of the initial guess is given by (6.39).

$$f_0 = 0.3318 \tag{6.39}$$

And the initial guess is depicted in Figure 28.

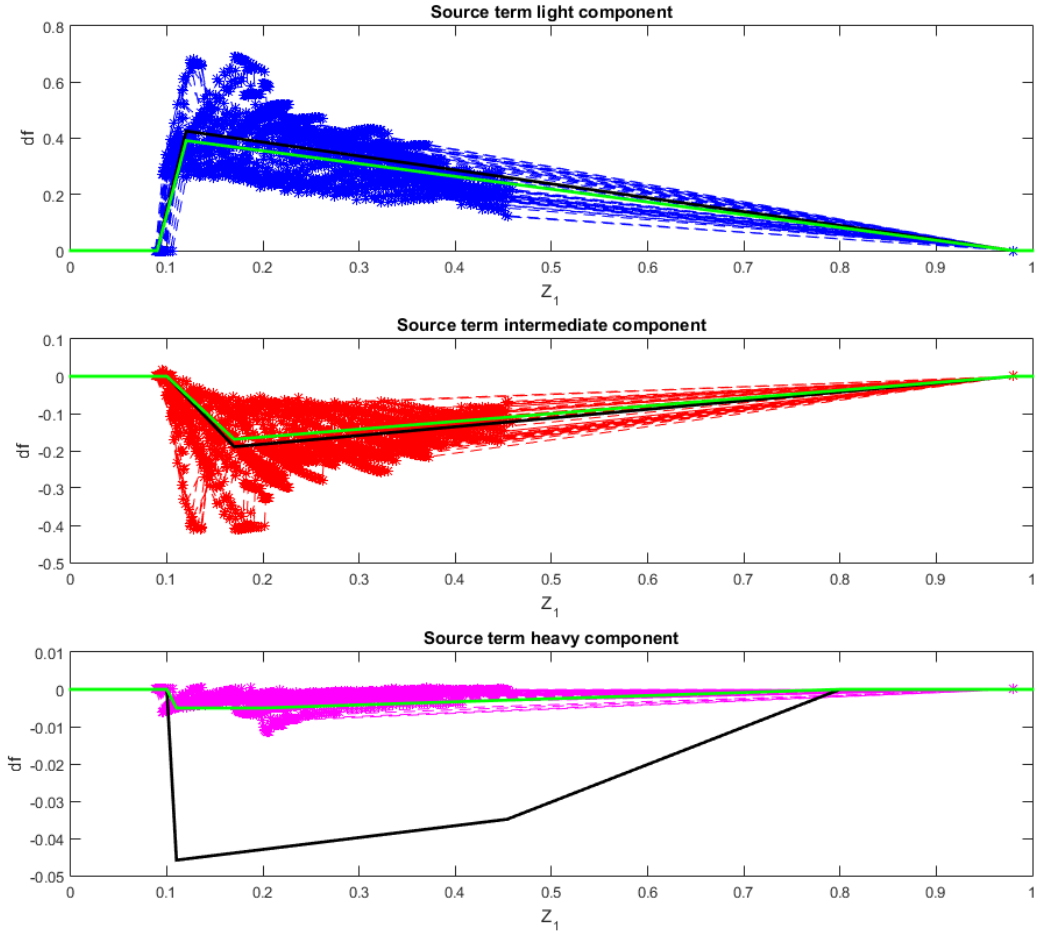

Figure 28 Source term graphs with initial guess correlation and optimized correlation for optimization 6.

Optimizing this initial guess results in the black line in Figure 28 and the saturation distribution shown by the black line in Figure 29. The misfit value from this optimization is given by (6.40).

$$f = 0.2473 \tag{6.40}$$

The values for the correlation are given by (6.41) and the used constraints for the parameters are given in (6.42) and (6.43).

$$\text{Fit} = [0.4257,\ -0.1891,\ -0.0458,\ 0.4537,\ -0.0349] \tag{6.41}$$

$$U_c = [1,\ 0,\ 0,\ 0.8,\ 0] \tag{6.42}$$

$$L_c = [0,\ -0.5,\ -0.1,\ 0.12,\ -0.1] \tag{6.43}$$

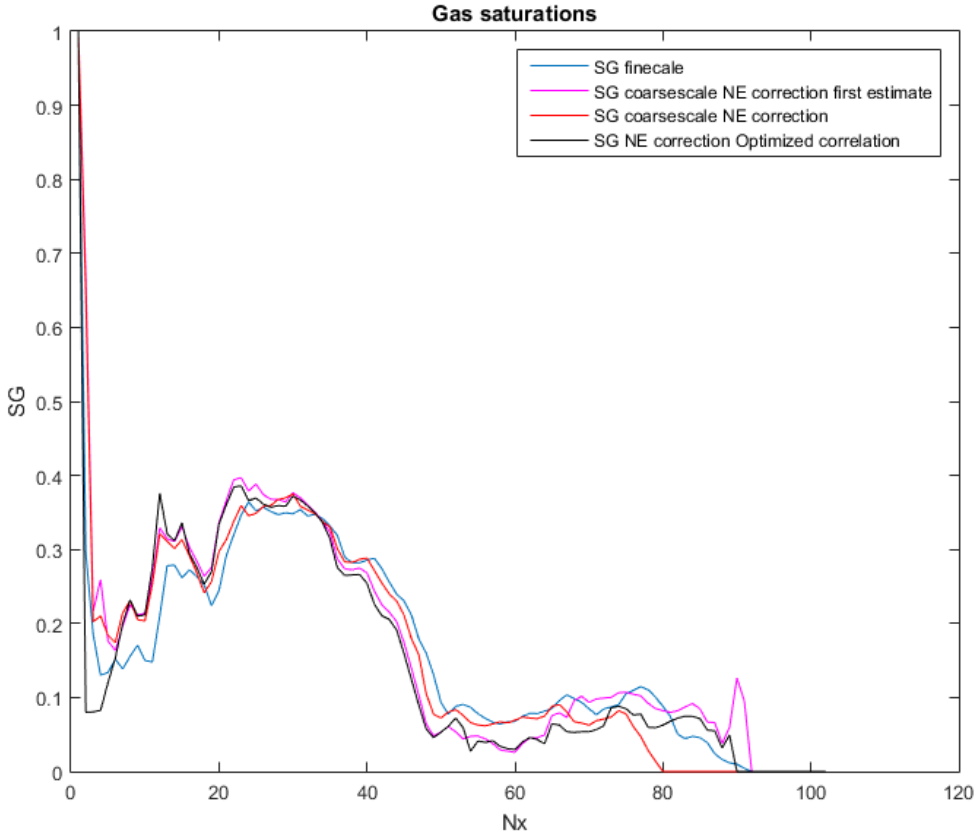

Figure 29 Saturation distribution comparison between the initial guess and correlation from optimization 6.

7 Conclusions and recommendations

In this chapter, the obtained results are discussed and some recommendations for further research are given.

7.1 Conclusions

The result of the effectively binary simulation show that the upscaling of the transmissibility and the relative permeabilities give an accurate coarse scale simulation result. Around grid block 70 the coarse scale result starts to deviate from the fine scale, but overall the result of the coarse simulation is satisfactory. When introducing thermodynamic effects to the simulation, an upscaling procedure for the composition is needed. The difference in gas saturation distributions between no correction for the thermodynamic effects and the Non-Equilibrium correction can clearly be seen in Figure 13. The simulation using the NE correction gives a more accurate result compared to the simulation without a correction for the thermodynamic effects. The misfit value f is significantly smaller when using the NE correction.

Finding a correlation between the source term df and the composition that works for all the grid blocks is difficult. The correlation shown in Figure 12 was created by finding a rough linear correlation for certain parts of the graph. Even though this correlation was created with this crude method, the resulting saturation distribution agreed well with the fine-scale average. Comparing the misfit values of the saturation distributions using the full df table and using the correlation, the correlation does give a less accurate result but is a big improvement on no correction at all. The misfit value for the correlation is in the same order of magnitude of the misfit value for the table.

Looking at Figure 14, the upscaling procedure works for the second permeability field as well. The saturation distribution using the source term table is slightly less accurate than for the first permeability distribution based on the misfit value. For the correlation the linear correlations does not seem sufficient and some parts should be replaced with a curved line. The misfit value for the saturation distribution from the simulation using the correlation is very high. This confirms that this correlation is not sufficient.

Because the correlations for the source term were only made roughly by hand, an optimization should improve the results. To cut down on calculation times a simple parameterization of the correlation was made. The results of the optimization procedures do improve on the initial guess and the first correlations from Figure 12 and Figure 15. However, adding parameters to the correlation for the third component did not improve the results significantly. The lack of improvement of the misfit by adding parameters to the correlation for the third component could indicate only a very small part of the correlation of the third component is of influence on the simulation results. The correlations for the first and second component could be of much bigger influence, but this was not investigated. The best optimized procedure gives a better result than using the values from the full df table based on the misfit value f.

Optimizing the result at t=60% does not seem to make a big difference and the optimization should work for the whole duration of the simulation, although the misfit appears to be increasing over time.

All the saturation distributions obtained with simulations using the correlations between the source term and composition have an inaccuracy compared to the simulation using the df table between roughly grid block 40 and 70. For the gird blocks between roughly 75 and 90, the correlations show a higher accuracy than the simulation using the df table.

To conclude, the non-equilibrium upscaling procedure proposed by Iranshahr, Chen [1] applied to the compositional equilibrium equation with K-values results in a high accuracy for the coarse scale simulation. The results obtained when using a correlation show it is possible to use this procedure without solving the global fine scale problem. However, this correlation can be improved further for improved results.

7.2 Recommendations

Based on this research and the results some recommendations can be made for further research. Since this research is based on a simple setup there are a lot of ways to expand the upscaling procedure for a more complicated setup. An obvious step would be to expand the procedure to a problem with a 2D coarse scale. This could be taken a step further to full 3D simulations. Another next step could be to increase the number of components. This complicates the simulations and might lead to longer calculation times, but it would show that this upscaling procedure is applicable on multiple problems. In this research, gravity and capillary effects are neglected, for a more complete physical model these should be included. However, including the gravity and capillary effects will lead to a much more complicated system. Both the fine scale and coarse scale simulations need to include gravity and capillary effects and an upscaling procedure is needed for the capillary effects.

Besides expanding on the case used in this research it is also a good idea to look at parts of the current setup. In this research, the upscaling for the relative permeabilities requires the full fine scale problem to be solved. Solving the full fine scale problem before upscaling does not lead to saving on calculation times by upscaling. A solution to this would be to find a correlation between the upscaled relative permeability and the saturation and create a upscaled relative permeability curve. This would be a similar solution to the correlation between the source term and composition made in this research. This will allow for parts of the reservoir to be solved on a fine scale to find the upscaled relative permeability curves which can then be used for the full reservoir. This solution can be examined much like the steps taken in this research for correlation between the source term and composition.

The correlation method for the source term is very crude in this research. It should be examined if a different correlation method can be used and if it leads to improved results. Additionally when a different correlation method is used a new optimization can be performed. The optimization procedure for the current correlations should be examined as well. In this research the optimization of the source term function primarily focused on optimizing the function for the third component. It is possible that further optimizing the function for the first and second component will lead to betterr improvements in the results.

Bibliography

1. Iranshahr, A., Y. Chen, and D.V. Voskov, *A coarse-scale compositional model.* Computational Geosciences, 2014. **18**(5): p. 797-815.
2. Glendasmith. 2013: PetroWiki.
3. Salehi, A., et al., *Upscaling of Compositional Flow Simulation Based on a Non-equilibrium Formulation*. 2016.
4. Durlofsky, L.J. *Upscaling and gridding of fine scale geological models for flow simulation.* in *8th International Forum on Reservoir Simulation Iles Borromees, Stresa, Italy*. 2005.
5. Deutsch, C., *Calculating Effective Absolute Permeability in Sandstone/Shale Sequences.*
6. Durlofsky, L.J., *Numerical calculation of equivalent grid block permeability tensors for heterogeneous porous media.* Water Resources Research, 1991. **27**(5): p. 699-708.
7. King, M.J. and M. Mansfield, *Flow Simulation of Geologic Models.*
8. Romeu, R.K. and B. Noetinger, *Calculation of Internodal Transmissivities in Finite Difference Models of Flow in Heterogeneous Porous Media.* Water Resources Research, 1995. **31**(4): p. 943-959.
9. Abbaszadeh, M. and N. Koide, *Evaluation of Permeability Upsealing Techniques and a New Algorithm for Interblock Transmissibilities*. Society of Petroleum Engineers.
10. Hou, T.Y. and X.-H. Wu, *A multiscale finite element method for elliptic problems in composite materials and porous media.* Journal of computational physics, 1997. **134**(1): p. 169-189.
11. Wu, X.-H., Y. Efendiev, and T.Y. Hou, *Analysis of upscaling absolute permeability.* Discrete and Continuous Dynamical Systems Series B, 2002. **2**(2): p. 185-204.
12. White, C.D. and R.N. Horne, *Computing Absolute Transmissibility in the Presence of Fine-Scale Heterogeneity*. Society of Petroleum Engineers.
13. Pickup, G., et al. *A method for calculating permeability tensors using perturbed boundary conditions*. in *ECMOR III-3rd European Conference on the Mathematics of Oil Recovery*. 1992.
14. Nielsen, B.F. and A. Tveito, *An upscaling method for one-phase flow in heterogeneous reservoirs. A weighted output least squares (WOLS) approach.* Computational Geosciences, 1998. **2**(2): p. 93-123.
15. Holden, L. and B.F. Nielsen, *Global Upscaling of Permeability in Heterogeneous Reservoirs; The Output Least Squares (OLS) Method.* Transport in Porous Media, 2000. **40**(2): p. 115-143.
16. Holden, L., B.F. Nielsen, and S. Sannan. *Upscaling of permeability using global norms*. in *ECMOR VII-7th European Conference on the Mathematics of Oil Recovery*. 2000.
17. Zhang, P., G.E. Pickup, and M.A. Christie, *A new practical method for upscaling in highly heterogeneous reservoir models.* SPE Journal, 2008. **13**(01): p. 68-76.
18. Chen, Y., B.T. Mallison, and L.J. Durlofsky, *Nonlinear two-point flux approximation for modeling full-tensor effects in subsurface flow simulations.* Computational Geosciences, 2008. **12**(3): p. 317-335.
19. Chen, Y. and Y. Li. *Incorporation of global effects in two-phase upscaling for modeling flow and transport with full-tensor anisotropy*. in *ECMOR XII-12th European Conference on the Mathematics of Oil Recovery*. 2010.
20. Chen, Y., et al., *A coupled local–global upscaling approach for simulating flow in highly heterogeneous formations.* Advances in Water Resources, 2003. **26**(10): p. 1041-1060.

21. Chen, Y. and L. Durlofsky, *Efficient Incorporation of Global Effects in Upscaled Models of Two-Phase Flow and Transport in Heterogeneous Formations.* Multiscale Modeling & Simulation, 2006. **5**(2): p. 445-475.
22. Chen, Y. and L.J. Durlofsky, *Adaptive Local–Global Upscaling for General Flow Scenarios in Heterogeneous Formations.* Transport in Porous Media, 2006. **62**(2): p. 157-185.
23. Chen, Y. and Y. Li, *Local-Global Two-Phase Upscaling of Flow and Transport in Heterogeneous Formations.* Multiscale Modeling & Simulation, 2009. **8**(1): p. 125-153.
24. Barker, J.W. and S. Thibeau, *A Critical Review of the Use of Pseudorelative Permeabilities for Upscaling.*
25. Barker, J.W. and P. Dupouy, *An analysis of dynamic pseudo-relative permeability methods for oil-water flows.* Petroleum Geoscience, 1999. **5**(4): p. 385-394.
26. Darman, N.H., G.E. Pickup, and K.S. Sorbie, *A Comparison of Two-Phase Dynamic Upscaling Methods Based on Fluid Potentials.* Computational Geosciences, 2002. **6**(1): p. 5-27.
27. Durlofsky, L.J. and Y. Chen, *Uncertainty Quantification for Subsurface Flow Problems Using Coarse-Scale Models*, in *Numerical Analysis of Multiscale Problems*, I.G. Graham, et al., Editors. 2012, Springer Berlin Heidelberg: Berlin, Heidelberg. p. 163-202.
28. Kyte, J.R. and D. Berry, *New pseudo functions to control numerical dispersion.* Society of Petroleum Engineers Journal, 1975. **15**(04): p. 269-276.
29. Stone, H. *Rigorous black oil pseudo functions*. in *SPE Symposium on reservoir simulation*. 1991. Society of Petroleum Engineers.
30. Wallstrom, T.C., et al., *Effective Flux Boundary Conditions for Upscaling Porous Media Equations.* Transport in Porous Media, 2002. **46**(2): p. 139-153.
31. Wallstrom, T.C., et al., *Application of Effective Flux Boundary Conditions to Two-Phase Upscaling in Porous Media.* Transport in Porous Media, 2002. **46**(2): p. 155-178.
32. Hui, M. and L. Durlofsky, *Accurate coarse modeling of well-driven, high-mobility-ratio displacements in heterogeneous reservoirs.* Journal of Petroleum Science and Engineering, 2005. **49**(1): p. 37-56.
33. Salehi, A., D.V. Voskov, and H.A. Tchelepi, *Thermodynamically Consistent Transport Coefficients for Upscaling of Compositional Processes*. Society of Petroleum Engineers.
34. Fayers, F., J. Barker, and T. Newley. *Effects of heterogeneities on phase behaviour in enhanced oil recovery*. in *ECMOR I-1st European Conference on the Mathematics of Oil Recovery*. 1989.
35. Barker, J. and F. Fayers, *Transport coefficients for compositional simulation with coarse grids in heterogeneous media.* SPE Advanced Technology Series, 1994. **2**(02): p. 103-112.
36. Camy, J. and A. Emanuel. *Effect of grid size in the compositional simulation of CO2 injection*. in *SPE Annual Fall Technical Conference and Exhibition*. 1977. Society of Petroleum Engineers.
37. Evazi, M. and K. Jessen, *Dual-Porosity Coarse-Scale Modeling and Simulation of Highly Heterogeneous Geomodels.* Transport in Porous Media, 2014. **105**(1): p. 211-233.
38. Zhang, B. and R. Okuno, *Modeling of capacitance flow behavior in EOS compositional simulation.* Journal of Petroleum Science and Engineering, 2015. **131**: p. 96-113.

39. Coats, K.H., L.K. Thomas, and R.G. Pierson, *Simulation of Miscible Flow Including Bypassed Oil and Dispersion Control.*
40. Christie, M.A. and P.J. Clifford, *Fast Procedure for Upscaling Compositional Simulation.*
41. Nghiem, L.X. and P.H. Sammon, *A Non-Equilibrium Equation-of-State Compositional Simulator*. Society of Petroleum Engineers.
42. Salehi, A., D.V. Voskov, and H.A. Tchelepi, *K-Values Based Non-Equilibrium Formulation for Upscaling of Compositional Simulation*. 2017, Society of Petroleum Engineers.
43. *AD-GPRS*. [Web page] [cited 2017; Available from: https://supri-b.stanford.edu/research-areas/ad-gprs.
44. Whitson, C. and M. L. Michelsen, *The Negative Flash*. Vol. 53. 1989. 51-71.
45. *MATLAB and Statistics Toolbox Release 2015a*. 2015, The MathWorks, Inc.: Natick, Massachusetts, United States.
46. Byrd, R.H., J.C. Gilbert, and J. Nocedal, *A trust region method based on interior point techniques for nonlinear programming.* Mathematical Programming, 2000. **89**(1): p. 149-185.
47. Byrd, R.H., M.E. Hribar, and J. Nocedal, *An Interior Point Algorithm for Large-Scale Nonlinear Programming.* SIAM Journal on Optimization, 1999. **9**(4): p. 877-900.
48. Waltz, R.A., et al., *An interior algorithm for nonlinear optimization that combines line search and trust region steps.* Mathematical Programming, 2006. **107**(3): p. 391-408.

Appendix A **Transmissibility conversion factor**

For the simulator the input units of transmissibility must be as given by (A.1)

$$T = \left[\frac{c_p \cdot m^3}{day \cdot bar} \right] \tag{A.1}$$

However, the units of permeability k_x and ΔX are given by (A.2)

$$\begin{aligned} k_i &= [mDarcy] \\ \Delta x, \Delta y, \Delta z &= [m] \end{aligned} \tag{A.2}$$

So without a conversion the units of (5.6) would be as given by (A.3)

$$T = [mDarcy \cdot m] \tag{A.3}$$

To find the conversion factor first all units will be transformed to SI units as shown in (A.4)

$$\begin{aligned} [m] &= [m] \\ [mDarcy] &= 9.869233 \cdot 10^{-16} \cdot [m^2] \\ [c_p] &= 10^{-3} \cdot [P_a \cdot s] \\ [day] &= 86400 \cdot [s] \\ [bar] &= 10^5 \cdot [P_a] \end{aligned} \tag{A.4}$$

$$\begin{aligned} [mDarcy \cdot m] &= 9.869233 \cdot 10^{-16} \cdot [m^3] \\ \left[\frac{c_p \cdot m^3}{day \cdot bar} \right] &= \frac{10^{-3}}{86400 \cdot 10^5} \cdot \left[\frac{P_a \cdot s \cdot m^3}{P_a \cdot s} \right] = 1.15740741 \cdot 10^{-13} \cdot [m^3] \end{aligned} \tag{A.5}$$

From this the conversion factor C_T can be calculated as (A.6)

$$C_T = \frac{9.869233}{1.15740741} \cdot \frac{10^{-16}}{10^{-13}} = 8.527017 \cdot 10^{-3} \tag{A.6}$$